



Published in final edited form as:

Cell Rep. 2018 November 20; 25(8): 2223–2233.e6. doi:10.1016/j.celrep.2018.10.100.

## Transmembrane Protease TMPRSS11B Promotes Lung Cancer Growth by Enhancing Lactate Export and Glycolytic Metabolism

Barrett L. Updegraff<sup>1</sup>, Xiaorong Zhou<sup>1,11</sup>, Yabin Guo<sup>1,13</sup>, Mahesh S. Padanad<sup>1</sup>, Pei-Hsuan Chen<sup>5,12</sup>, Chendong Yang<sup>5</sup>, Jessica Sudderth<sup>5</sup>, Carla Rodriguez-Tirado<sup>1</sup>, Luc Girard<sup>3,8</sup>, John D. Minna<sup>3,4,8</sup>, Prashant Mishra<sup>2,5</sup>, Ralph J. DeBerardinis<sup>2,5,6,10</sup>, and Kathryn A. O'Donnell<sup>1,7,9,14,\*</sup>

<sup>1</sup>Department of Molecular Biology, University of Texas Southwestern Medical Center, Dallas, TX 75390-9148, USA

<sup>2</sup>Department of Pediatrics, University of Texas Southwestern Medical Center, Dallas, TX 75390, USA

<sup>3</sup>Department of Pharmacology, University of Texas Southwestern Medical Center, Dallas, TX 75390-8593, USA

<sup>4</sup>Department of Internal Medicine, University of Texas Southwestern Medical Center, Dallas, TX 75390-8593, USA

<sup>5</sup>Children's Medical Center Research Institute, University of Texas Southwestern Medical Center, Dallas, TX 75390, USA

<sup>6</sup>McDermott Center for Human Growth and Development, University of Texas Southwestern Medical Center, Dallas, TX 75390, USA

<sup>7</sup>Harold C. Simmons Comprehensive Cancer Center, University of Texas Southwestern Medical Center, Dallas, TX 75390, USA

<sup>8</sup>Hamon Center for Therapeutic Oncology Research, University of Texas Southwestern Medical Center, Dallas, TX 75390-8593, USA

<sup>9</sup>Hamon Center for Regenerative Science and Medicine, University of Texas Southwestern Medical Center, Dallas, TX 75390-9148, USA

<sup>10</sup>Howard Hughes Medical Institute, University of Texas Southwestern Medical Center, Dallas, TX 75390, USA

<sup>11</sup>Department of Immunology, Nantong University School of Medicine, Nantong 226001, China

<sup>12</sup>Department of Cancer Biology, Dana-Farber Cancer Institute, Boston, MA 02115, USA

This is an open access article under the CC BY-NC-ND license.

\*Correspondence: kathryn.odonnell@utsouthwestern.edu.

### AUTHOR CONTRIBUTIONS

Conception and Design, K.A.O. and B.L.U.; Data Acquisition, B.L.U., X.Z., Y.G., M.S.P., P.-H.C., C.Y., J.S., and C.R.-T.; Analysis and Interpretation of Data, K.A.O., B.L.U., L.G., Y.G., M.S.P., J.D.M., R.J.D., and P.M.; Writing and Revision of Manuscript, K.A.O., B.L.U., J.D.M., R.J.D., M.S.P., and P.M.; Funding Acquisition, K.A.O., B.L.U., J.D.M., and R.J.D.

### DECLARATION OF INTERESTS

The authors declare no competing interests.



## INTRODUCTION

Tumor cells acquire and metabolize glucose at rates far exceeding their mitochondrial oxidative capacity (Hanahan and Weinberg, 2011). This enhanced flux allows for shunting of glycolytic intermediates toward biosynthetic pathways to meet the proliferative demands of rapidly dividing tumor cells (DeBerardinis et al., 2008). Most pyruvate from glycolysis is reduced to lactate by lactate dehydrogenase (LDH) and ex-ported from the cell through the dedicated H<sup>+</sup>-coupled monocar-boxylate transporters MCT1 and MCT4 (encoded by *SLC16A1* and *SLC16A3*, respectively) (Dimmer et al., 2000; Halestrap and Price, 1999; Warburg et al., 1927). This reduction of pyruvate to lactate regenerates NAD<sup>+</sup>, which facilitates flux through the glycolytic pathway. Co-transport of protons generated from this reaction with lactate through MCTs is also critical for maintenance of appropriate intracellular pH. In tumors, impairing MCT4-mediated lactate export disrupts tumor pH, tumor growth, and glycolytic flux (Le Floch et al., 2011). In some systems, MCT1 drives lactate uptake and fuels mitochondrial oxidation (Sonveaux et al., 2008), whereas MCT4 favors lactate export and is upregulated during hypoxia and in highly glycolytic tissues (Dimmer et al., 2000; Ullah et al., 2006; Bonen, 2001). These transporters therefore orchestrate diverse metabolic responses to oxygen and nutrient availability in human tumors (Hensley et al., 2016).

Several observations contribute to our knowledge of lactate metabolism in both normal physiology and pathological contexts. Tumor-derived lactate has been shown to blunt immune cell proliferation and effector function through acidification of the microenvironment and upregulation of tumor PD-L1 expression (Feng et al., 2017; Fischer et al., 2007). Moreover, the lactate content of tumors is positively correlated with radiation resistance, metastasis, and patient mortality (Quennet et al., 2006; Sattler et al., 2010; Walenta et al., 2000). This large carbon pool was initially thought to be solely a glycolytic waste product. However, in human lung tumors, it was shown that imported lactate contributes more than twice as many tricarboxylic acid (TCA) cycle carbons as pyruvate immediately derived from glycolysis (Faubert et al., 2017). These studies suggest that manipulation of lactate production or transport is a vulnerability that may be exploited for therapeutic targeting of cancer cells.

Cell surface expression of MCT1 and MCT4 is facilitated by the transmembrane glycoprotein Basigin/CD147 (Kirk et al., 2000). In addition to important roles in development, Basigin is expressed highly across numerous cancer types and has been shown to promote tumor growth and metastasis (Hori et al., 2000; Igakura et al., 1998; Zucker et al., 2001). However, the mechanisms through which Basigin promotes tumorigenesis remain incompletely understood, with reports implicating its interactions with extracellular matrix (ECM) factors, regulation of matrix metalloproteases (MMPs), and hyaluronan production (Marieb et al., 2004; Kanekura et al., 2002). Basigin plays a well-established role in trafficking MCTs to the plasma membrane for proper function (Yurchenko et al., 2002; Li et al., 2001; Marieb et al., 2004; Izumi et al., 2003). In this study, we describe the unexpected finding that a poorly characterized transmembrane serine protease TMPRSS11B promotes Basigin/MCT4-mediated lactate export. TMPRSS11B belongs to the differentially expressed in squamous cell cancer (DESC) family of genomically clustered trypsin-like serine

proteases that share commonality in their type II transmembrane insertion, catalytic triad spacing, and disulfide bonding anchoring their serine protease domain to a membrane proximal cysteine (Bugge et al., 2009). Using extracellular factor profiling coupled with metabolomics, we demonstrate that *TMPRSS11B* promotes cell surface expression and solubilization of Basigin and that this enhances the efficiency of MCT4-mediated lactate export, glycolytic flux, and tumor growth. Collectively, this work identifies an oncogenic transmembrane protease that promotes tumorigenesis, thereby uncovering an enzymatic activity that may be targeted for cancer therapy.

## RESULTS

To identify genes that promote transformation of human bronchial epithelial cells (HBECs), we performed *Sleeping Beauty* (*SB*)-mediated transposon mutagenesis of immortalized HBECs stably expressing CDK4, human telomerase reverse transcriptase (hTERT), and short hairpin RNA (shRNA) targeting *TP53* (HBEC-shp53). These cells progress to full malignancy upon overexpression of oncogenes such as *KRAS*<sup>G12V</sup> and *MYC* (Sato et al., 2013). We transfected cells with the mutagenic *T2/Onc* transposon and the *SB100* transposase, as previously described (Guo et al., 2016). Following *SB* mutagenesis, transformation was assessed by the ability to efficiently form large colonies in soft agar. Genomic DNA extracted from ~300 large colonies served as a template for ligation-mediated PCR (LM-PCR) followed by deep sequencing to identify transposon insertions. Common insertion site (CIS) analysis was then performed, revealing candidate genes that may promote transformation in this system (Table S1). Among the putative oncogenes identified in this screen, we were particularly interested surface proteins, because they might represent therapeutic targets that are accessible to antibody-based therapies. One of the identified CIS genes encodes the transmembrane serine protease *TMPRSS11B*, which lacks known physiological substrates. Several *TMPRSS11* family members were identified in the screen, and we selected *TMPRSS11B* as a representative family member for functional studies. We found that *TMPRSS11B* expression is highly upregulated in lung squamous cell carcinoma (LSCC) compared to normal lung tissue or other subtypes of non-small cell lung cancer (NSCLC), including adenocarcinoma (Figure S1A). Moreover, high expression of *TMPRSS11B* mRNA correlated with poor overall survival in NSCLC patients, warranting further investigation of the role of this enzyme in tumorigenesis (Figure S1B) (Lee et al., 2008).

### **TMPRSS11B Promotes Transformation and Tumorigenesis**

To confirm that *TMPRSS11B* promotes transformation of bronchial epithelial cells, we stably expressed the protein in HBECshp53 cells and assessed colony formation. To test whether catalytic function is necessary for transforming activity, we mutated residues in the catalytic triad of this family of proteases (D270N and S366A) (Figure 1A) (Miller et al., 2014). Expression of V5-tagged *TMPRSS11B* proteins was confirmed by western blotting (Figure S2A). The S366A mutation resulted in faster migration of the protein, consistent with disruption of a nearby N-linked glycosylation site (Figures S2A and S2B). Expression of wild-type *TMPRSS11B* robustly stimulated anchorage-independent growth, and this effect was strongly impaired by the catalytic mutations (Figure 1B). Moreover, stable

ectopic expression of *TMPRSS11B* enhanced proliferation of HBECshp53 cells (Figure S2C) and promoted growth in soft agar in several human LSCC lines (Figure 1C). These data suggest that *TMPRSS11B* exhibits oncogenic activity in lung epithelial and LSCC cells.

To determine whether inhibition of *TMPRSS11B* limits tumor growth, we performed loss-of-function studies using shRNA-mediated knockdown and CRISPR-mediated genome editing. First, lentivirally delivered shRNA was used to deplete *TMPRSS11B* in the LSCC lines HCC2814 and H157 and the prostate cancer line DU145 (Figure 1D), which expressed high levels of *TMPRSS11B* mRNA (Barretina et al., 2012). Xenograft assays in immunocompromised non-obese diabetic/severe combined immunodeficiency (NOD/SCID)  $Il2rg\gamma^{-/-}$  (NSG) mice demonstrated a strong impairment of tumorigenesis following depletion of *TMPRSS11B* in each of these cell lines (Figures 1E–1G; Figure S2D). To confirm these findings, we mutated the endogenous *TMPRSS11B* locus using CRISPR-mediated genome editing in HCC2814 cells. Again, this resulted in greatly reduced tumor growth, an effect that could be rescued by ectopic expression of *TMPRSS11B* (Figure 1H). Altogether, these data demonstrate that inhibition of *TMPRSS11B* impairs tumorigenesis, raising the possibility that targeting *TMPRSS11B* may provide a therapeutic strategy in LSCC.

### **TMPRSS11B Promotes Solubilization of Basigin**

Given that *TMPRSS11B* harbors an extracellular (EC) protease domain, we hypothesized that proteolysis of a membrane-bound substrate may underlie its transforming activity. To identify candidate substrates of *TMPRSS11B*, a set of soluble receptors was interrogated using proteome profiler arrays with conditioned media (CM) from HBEC-shp53 cells with or without *TMPRSS11B* overexpression. This revealed an ~10-fold enrichment in the levels of soluble Basigin/CD147 in conditioned media from cells expressing *TMPRSS11B* (Figures 2A and 2B). Through the analysis of HBEC-shp53 cells expressing wild-type *TMPRSS11B* or two catalytic mutants, we confirmed that expression of proteolytically active *TMPRSS11B* results in Basigin solubilization (Figure 2C). *TMPRSS11B* overexpression in HCC95 and HCC1313 LSCC cells also stimulated Basigin release (Figure 2D). shRNA-mediated inhibition of *TMPRSS11B* or treatment with the irreversible serine protease inhibitor 4-(2-aminoethyl)benzene-sulfonyl fluoride (AEBSF) reduced Basigin solubilization in a dose-dependent manner (Figures 2E and 2F). Moreover, AEBSF treatment of LSCC and lung adenocarcinoma cells reduced Basigin release (Figure 2G). Overall Basigin mRNA and protein expression was similar in control and *TMPRSS11B*-expressing cells (Figures S3A–S3D). Furthermore, similar levels of Basigin mRNA and protein were observed in LSCC cells with control and *TMPRSS11B* shRNA and in AEBSF-treated HBEC-shp53 cells (Figures S3E–S3H).

Previous studies have shown that Basigin stimulates proliferation (Arendt et al., 2014; Su et al., 2009). We therefore assessed whether released Basigin could non-cell-autonomously enhance proliferation of HBEC-shp53 cells. Conditioned media from HBEC-shp53 cells expressing GFP, *TMPRSS11B*-D270N, *TMPRSS11B*-S366A, or WT *TMPRSS11B* were transferred to untransfected HBEC-shp53 cells. No difference in proliferation was observed,

suggesting that released Basigin in conditioned media does not stimulate proliferation in this system(Figure S3I).

### **TMPRSS11B Interacts with Basigin and MCT4 at the Plasma Membrane**

We next assessed interactions among TMPRSS11B, Basigin, and MCT4 by performing reciprocal co-immunoprecipitations in HBEC-shp53 and HCC2814 cells expressing tagged TMPRSS11B and Basigin constructs. Co-immunoprecipitation Revealed interactions between hemagglutinin (HA)-tagged TMPRSS11B and V5-tagged Basigin and between V5-tagged TMPRSS11B and endogenous MCT4 (Figures 3A and 3B). We confirmed the interaction between V5-tagged TMPRSS11B and endogenous Basigin in HCC2814 cells by co-immunoprecipitation with three independent antibodies (Figure 3C).

Immunofluorescence confocal microscopy revealed substantial co-localization of TMPRSS11B, MCT4, and Basigin at the plasma membrane of HBEC-shp53 cells (Figures 3D and 3E; Figure S4A). These data demonstrate that TMPRSS11B interacts with Basigin and MCT4 at the plasma membrane.

Immunofluorescence staining showed modest alterations in Basigin localization upon TMPRSS11B loss of function. TMPRSS11B knockdown in HCC2814 cells resulted in less distinct membrane staining of Basigin relative to control cells (Figure S4B). Total levels of cellular Basigin remain unchanged in these cells (Figure S3F), suggesting that TMPRSS11B may influence trafficking of Basigin to the plasma membrane.

### **TMPRSS11B Promotes Lactate Export**

To investigate the role of Basigin downstream of TMPRSS11B, CRISPR/Cas9 was used to generate clonal HBEC-shp53-*TMPRSS11B* cells with Basigin (*BSG*) knockout. This led to decreased protein levels of MCT1 and MCT4, consistent with earlier reports demonstrating the essential chaperone function of Basigin for these lactate transporters (Figure S5A) (Philp et al., 2003). Moreover, Basigin and MCT4 are expressed similarly in control HBEC-shp53-GFP and HBEC-shp53-TMPRSS11B cells (Figure S3B), suggesting that membrane release of Basigin mediated by TMPRSS11B does not alter MCT4 expression. Next, we monitored the effects of Basigin depletion in HBEC-shp53 lacking TMPRSS11B by generating CRISPR/Cas9-edited clones (Figure S5B). Basigin knockout in these cells had no appreciable effect on proliferation (Figure 4A). However, stable expression of TMPRSS11B failed to significantly stimulate proliferation in Basigin knockout cells (Figure 4A), and TMPRSS11B-mediated anchorage-independent growth was reduced (Figure 4B). These data demonstrate that Basigin knockout is tolerated in HBEC-shp53 cells and that TMPRSS11B-mediated proliferation and transformation are facilitated by Basigin in this system.

Given the critical role for Basigin in MCT1 and MCT4 trafficking, we hypothesized that Basigin solubilization might regulate MCT1 and MCT4-mediated lactate transport function. Consistent with this hypothesis, intracellular lactate quantification revealed an ~25% reduction in steady-state lactate content of HBEC-shp53-*TMPRSS11B* compared with control HBEC-shp53-GFP cells (Figure 4C). This reduction was reversed in independent *BSG* knockout clones and partially reversed in HBEC-shp53-TMPRSS11B cells treated with AEBSF (Figure 4C). To rule out the possibility that this reduction in steady-state intracellular

lactate levels was due to a defect in glucose uptake and therefore reduced glycolytic flux, we measured uptake of the fluorescent glucose analog (2-(*N*-(7-Nitrobenz-2-oxa-1,3-di-azol-4-yl)Amino)-2-Deoxyglucose) (2-NBDG). No significant difference between HBEC-shp53-TMPRSS11B and HBEC-shp53 control cells was observed (Figure S5C). Extracellular flux analysis demonstrated that TMPRSS11B enhanced extracellular acidification rates (ECARs), a readout of glycolytic flux and a commonly used proxy for lactate secretion (Figure 4D). The enhanced export was reduced in independent Basigin knockout (KO) clones and rescued in cells by reintroduction of a CRISPR/Cas9-resistant Basigin construct (Figure 4D). Moreover, in separate Basigin KO cells lacking TMPRSS11B expression, we found only a modest (~10%) reduction in ECAR compared with control non-targeting guide RNA (gRNA) (sgNS) cells, suggesting that Basigin KO is tolerated in HBEC-shp53 cells (Figure 4E). This may reflect a vulnerability of TMPRSS11B-expressing cells to Basigin KO that is not observed in syngeneic cells lacking TMPRSS11B. To distinguish between the roles of MCT1 and MCT4 in this system, we compared HBEC-shp53-TMPRSS11B cells with either MCT4 deletion or treatment with the chemical MCT1 inhibitor SR13800 and observed that ECAR was reduced dramatically in MCT4 KO cells but minimally upon MCT1 inhibition (Figure 4F; Figure S5D). Altogether, these findings provide evidence that TMPRSS11B enhances the lactate transport efficiency of Basigin/MCT4 complexes in HBEC-shp53 cells.

### Depletion of TMPRSS11B Reduces Lactate Export

To demonstrate its role in promoting lactate export, TMPRSS11B was depleted using shRNA in the LSCC lines HCC2814, H157, and HCC95 and the prostate cancer line DU145. CRISPR-mediated genome editing was used to mutate the endogenous *TMPRSS11B* locus in polyclonal populations of the lung adenocarcinoma cell line H2073 and in clonal lines of HCC2814 cells (Figure S5E; Table S2). TMPRSS11B reduction in these cells resulted in an 0.3- to 3.5-fold increase in intracellular lactate levels (Figure 5). Increased intracellular lactate in *TMPRSS11B* KO clones was specifically due to TMPRSS11B loss of function, because restoring TMPRSS11B expression with cDNA harboring silent mutations in the single guide RNA (sgRNA) targeting site led to a significant reduction in intracellular lactate levels (Figure 5G). We confirmed that these cells consume similar amounts of 2-NBDG (Figure S6), ruling out the possibility that this lactate accumulation is caused by enhanced glucose uptake.

To monitor the metabolic consequences of TMPRSS11B inhibition, we performed [1,6-<sup>13</sup>C]glucose tracing in HCC2814 cells with shRNA-mediated TMPRSS11B knockdown and observed a reduction in lactate<sup>m+1</sup> export (Figure S7A) in the same cells in which we documented significant accumulation of steady-state intracellular lactate (Figure 5A). Overall, our findings suggest that TMPRSS11B in LSCC enhances tumorigenesis by facilitating lactate export.

RNA sequencing (RNA-seq) was used to assess the cellular consequences of TMPRSS11B gain of function (GOF) (HBEC-shp53-GFP versus HBEC-shp53-TMPRSS11B) and loss of function (LOF) (HCC2814-EV and HCC2814-sh *TMPRSS11B*). In TMPRSS11B-overexpressing cells, Database for Annotation, Visualization, and Integrated Discovery

(DAVID) pathway analysis of significantly upregulated genes retrieved metabolic pathways as the top hit ( $p < 0.05$ , false discovery rate [FDR]  $< 0.1$ ) (Figure S7B). We also assessed levels of transcripts in pathways involved in glucose metabolism. This revealed subtle yet consistent upregulation of genes involved in glucose uptake, glycolysis, the pentose phosphate pathway (PPP), and the TCA cycle following *TMPRSS11B* overexpression and downregulation of these pathways following *TMPRSS11B* loss of function (Figure S7C). This poses the intriguing possibility that enhanced lactate export also induces a transcriptional program favoring a metabolic shift toward aerobic glycolysis and that this may function to bolster the proliferative capacity of cells. This is in agreement with earlier studies demonstrating that depletion of MCT4, Basigin, or both induces lactate accumulation and slows glycolytic flux (Marchiq et al., 2015). In addition to enhancing glycolytic ECAR, overexpression of *TMPRSS11B* significantly enhanced the oxygen consumption rate (OCR) (Figure S7D), consistent with a report demonstrating that transported lactate contributes to the TCA cycle carbon pool more than pyruvate directly derived from glycolysis (Faubert et al., 2017).

Finally, we determined whether expression of *TMPRSS11B* or its other family members correlated with lactate secretion in cultured human LSCCs. Rates of lactate secretion were measured in a panel of NSCLC cell lines, including 12 cell lines derived from LSCC. The lactate secretion rate was then correlated with transcript abundance for each of the *TMPRSS11* family members. *TMPRSS11B* mRNA, but none of the other *TMPRSS11* family members, positively correlated with lactate secretion (Figure 6), suggesting *TMPRSS11B* acts non-redundantly to enhance lactate secretion.

## DISCUSSION

To identify genes that promote transformation of HBECs, we performed an unbiased forward genetic screen and identified putative oncogenes and tumor suppressors relevant to lung cancer pathogenesis. We were particularly interested in cell surface proteins, because they may represent therapeutic targets that are accessible to antibody-based therapies. These efforts revealed that overexpression of the transmembrane serine protease *TMPRSS11B* promotes transformation in this system. *TMPRSS11B* is highly expressed in LSCC tumors and is associated with poor clinical outcomes. *TMPRSS11B* overexpression induces cellular transformation *in vitro*, while depletion of *TMPRSS11B* reduces the tumor growth of LSCC and prostate cancer cells in mice, supporting an oncogenic function for this protein in tumorigenesis. Our mechanistic studies support a model whereby *TMPRSS11B* interacts with and promotes Basigin solubilization, resulting in enhanced MCT4-mediated lactate export. Consequently, this increases glycolytic flux and tumor growth (Figure 7). These results, coupled with *TMPRSS11B* being an enzyme localized to the cell membrane, raise the possibility that this protein may be targeted with therapeutic antibodies or small molecules in LSCC and other malignancies. Moreover, these findings further our understanding of the function and regulation of Basigin, a protein that is known to act as an essential chaperone for cell surface expression of the lactate transporters MCT1 and MCT4.

Studies have demonstrated that human lung tumors, as well as most healthy tissues in the body, use circulating lactate to fuel TCA cycle oxidation, suggesting that glycolytic flux is

uncoupled from TCA cycle flux at the level of pyruvate reduction to lactate and that enhancing lactate secretion may fuel cellular respiration non-autonomously (Hui et al., 2017; Faubert et al., 2017). Moreover, clinical progression of post-operative NSCLC patients correlated with tumor lactate uptake and oxidation in a manner dependent on MCT1 in experimental NSCLC tumors (Faubert et al., 2017). These findings underscore the importance of investigating mechanisms of lactate transport to develop novel therapies that target this process.

TMPRSS11B may regulate Basigin through multiple possible non-mutually exclusive mechanisms, including direct proteolytic cleavage, as well as enhanced Basigin secretion. Consistent with the latter possibility, MCT4 and Basigin have been found in secreted vesicles purified from the sera of prostate cancer patients and in conditioned media of human ovarian and breast carcinoma cell lines (Gallagher et al., 2007; Millimaggi et al., 2007; Yoshioka et al., 2014). Metabolic profiling of exosomal vesicles isolated from prostate cancer patients revealed higher concentrations of lactate than any other metabolite measured (Zhao et al., 2016). In addition, flux analysis in cultured cells revealed substantial rates of labeled lactate secretion via exosomes and uptake of exosomal lactate by recipient cells (Achreja et al., 2017). This raises the intriguing possibility of vesicular export of lactate, in which the pH gradient between cytosol and Golgi secretory compartments, along with the topological orientation of Basigin and MCT4, would favor the import of lactate into vesicles (Achreja et al., 2017; Zhao et al., 2016). Moreover, Basigin-decorated vesicles are subject to regulated endosomal recycling through clathrin-independent endocytosis (Maldonado-Báez et al., 2013). Our data demonstrating reduced plasma membrane localization of Basigin upon TMPRSS11B loss of function is consistent with this hypothesis. Nevertheless, proteolysis is likely a key component of the relevant TMPRSS11B mechanism given our data demonstrating the reduced transforming activity and Basigin solubilization by TMPRSS11B catalytic mutants. Thus, while our findings have uncovered a previously unrecognized TMPRSS11B-Basigin regulatory interaction that is crucial for lactate metabolism and secretion in cancer cells, important mechanistic questions remain for future investigation.

Our study expands our understanding of the metabolic alterations that contribute to tumor progression in LSCC. Yet the mechanism by which TMPRSS11B is upregulated in LSCC is unknown. In a mouse model of LSCC with homozygous deletion of *Pten* and *Stk11* (Lkb1), the mouse ortholog of *TMPRSS11B*, *Tmprss11bnl*, is among the top 20 upregulated genes in tumors, hinting at a conserved mechanism of tumor metabolic regulation (Xu et al., 2014). Physiological TMPRSS11B expression is largely restricted to cervical and esophageal tissue (GTEx Consortium, 2013) but is highly upregulated in LSCC and other squamous cell carcinomas (Gao et al., 2013), while Basigin and MCT4 are expressed highly throughout the body in tissues such as erythrocytes, brain, skeletal muscle, and activated immune populations. This suggests that therapies targeting TMPRSS11B may be more specific to tumor cells and result in fewer side effects and less toxicity compared to Basigin or MCT4 inhibitors (Halestrap and Price, 1999). Additional studies are warranted to identify substrates of TMPRSS11B in both physiological and pathophysiological settings. Given that this cell surface protein is also an enzyme, small molecules or antibodies directed against the site of catalysis may be developed to inhibit TMPRSS11B function in future studies

## STAR+METHODS

Author Manuscript

Author Manuscript

Author Manuscript

Author Manuscript

## KEY RESOURCES TABLE

REAGENT or RESOURCE	SOURCE	IDENTIFIER
<b>Antibodies</b>		
Rabbit anti-human Basigin (E1S1V)	Cell Signaling Technology	Cat. # 13287S
Mouse anti-human Basigin (1S9–2A)	Millipore Sigma	Cat. # MAB2623; RRID:AB_11212827
Mouse anti-human Basigin (MEM/M6–6)	Abcam	Cat. # ab119114; RRID:AB_2274970
Mouse anti-human Basigin (MEM/M6–1)	Abcam	Cat. # ab666; RRID:AB_1508093
Mouse anti-human Basigin (MEM/M6–6)	ThermoFisher	Cat. # MA1–10103; RRID:AB_2274970
Rabbit anti-beta-Actin (13E5)	Cell Signaling Technology	Cat. # 4970S
Rabbit anti-HA (C29F4)	Cell Signaling Technology	Cat. # 3724S
Mouse anti-HA (HA-7)	Millipore Sigma	Cat. # H3663; RRID:AB_262051
Rat anti-HA (3F10)	Millipore Sigma	Cat. # 11867423001; RRID:AB_390918
Mouse anti-MCT1 (H-1)	Santa Cruz Biotechnology	Cat. # sc-365501; RRID:AB_10841766
Mouse anti-MCT4 (D-1)	Santa Cruz Biotechnology	Cat. # sc-376140; RRID:AB_10992036
Rabbit anti-MCT4 (polyclonal, Prestige)	Millipore Sigma	Cat. # HPA021451; RRID:AB_1853663
Mouse anti-Tubulin (DM1A)	Abcam	Cat. # ab7291; RRID:AB_2241126
Mouse anti-V5	ThermoFisher	Cat. # R960–25; RRID:AB_2556564
Rabbit anti-V5 (D3H8Q)	Cell Signaling Technology	Cat. # 13202S
Goat anti-mouse-Alexa Flour 488	Cell Signaling Technology	Cat. # 4408S; RRID:AB_2576208
Goat anti-rabbit-Alexa Flour 488	Cell Signaling Technology	Cat. # 4412S; RRID:AB_2630356
Goat anti-rabbit-Alexa Flour 594	Cell Signaling Technology	Cat. # 8889S; RRID:AB_2650602
Goat anti-rat-Alexa Flour 647	Cell Signaling Technology	Cat. # 4418S; RRID:AB_2566823
Horse anti-mouse-IgG HRP secondary	Cell Signaling Technology	Cat. # 7076S
Goat anti-rabbit-IgG HRP secondary	Cell Signaling Technology	Cat. # 7074S
<b>Bacterial and Virus Strains</b>		
OneShot Stbl3 <i>E. coli</i>	ThermoFisher	Cat. # C737303
Lentivirus: LX303	This paper	Addgene 25897
Lentivirus: LX307	This paper	N/A
Lentivirus: LentiCRISPRv2	This paper	Addgene 52961
Lentivirus: TRIPZ	This paper	Cat. # RHS4696
<b>Biological Samples</b>		

REAGENT or RESOURCE	SOURCE	IDENTIFIER
Xenograft tumor tissue: HCC2814 Lung sq. cell carcinoma (M)	This paper	Cell line: RRID:CVCL_V586
Xenograft tumor tissue: H157 Lung sq. cell carcinoma (M)	This paper	Cell line: RRID:CVCL_0463
Xenograft tumor tissue: DU145 Prostate carcinoma (M)	This paper	Cell line: RRID:CVCL_0105
Chemicals, Peptides, and Recombinant Proteins		
SR13800 (MCT1 inhibitor)	Millipore Sigma	Cat. # 509663
Oligomycin	Millipore Sigma	Cat. # 75351
[1,6- <sup>13</sup> C] glucose	Millipore Sigma	Cat. # 453196
Pefabloc SC AEBSF (Serine protease inhibitor)	Millipore Sigma	Cat. # 11429868001
Doxycycline hyclate	Millipore Sigma	Cat. # D9891
Hexadimethrine bromide	Millipore Sigma	Cat. # 107689
Fetal bovine serum (FBS)	Millipore Sigma	Cat. # F2442
Puromycin dihydrochloride	ThermoFisher	Cat. # A1113803
Blasticidin S HCl	ThermoFisher	Cat. # A1113903
2-NBDG	ThermoFisher	Cat. # N13195
HALT Protease Inhibitor Cocktail	ThermoFisher	Cat. # 78430
NuPAGE LDS Sample Loading Buffer	ThermoFisher	Cat. # NP0008
NuPAGE Sample Reducing Agent	ThermoFisher	Cat. # NP0004
Bolt 4–12% Bis-Tris Plus Gels	ThermoFisher	Cat. # NW04120BOX
Phusion Site-Directed Mutagenesis Kit	ThermoFisher	Cat. # F541
Gateway LR Clonase II Enzyme Mix	ThermoFisher	Cat. # 11791100
SuperScript IV VILO RT Master Mix	ThermoFisher	Cat. # 11756050
Hanks Balanced Salt Solution, no magnesium, no calcium, no phenol red (HBSS-)	ThermoFisher	Cat. 14175103
Keratinocyte Serum-Free Medium (KSFM)	ThermoFisher	Cat. # 17005042
RPMI-1640 medium	ThermoFisher	Cat. # A1049101
RPMI-1640 medium, glucose/bicarbonate-free	ThermoFisher	Cat. # R1383
Leibovitz's L-15 medium, no phenol red	ThermoFisher	Cat. # 21083027
Lysis Buffer LB-17	R&D Systems	Cat. # 895943
Lenti-X Concentrator	Clontech	Cat. # 631232
Effectene Transfection Reagent	QIAGEN	Cat. # 301427
RNeasy Mini Kit	QIAGEN	Cat. # 74106
Critical Commercial Assays		
sReceptor Proteome Profiler Array	R&D Systems	Cat. # ARY012
EMMPRIN/CD147 Quantikine ELISA	R&D Systems	Cat. # DEMP00
Lactate Assay Kit	Millipore Sigma	Cat. # MAK064
TaqMan Universal qPCR Master Mix	ThermoFisher	Cat. # 4304437
Dynabeads Protein G Immunoprecipitation Kit	ThermoFisher	Cat. # 10007D

REAGENT or RESOURCE	SOURCE	IDENTIFIER
Pierce BCA Protein Assay Kit	ThermoFisher	Cat. # 23225
SeaKem LE Agarose	Lonza	Cat. # 50004
Deposited Data		
RNA sequencing data and analysis	NCBI GEO	GSE114850
Experimental Models: Cell Lines		
Human – HBEC-3KT (F)	(Ramirez et al., 2004)	RRID:CVCL_EQ78
Human - HCC95 Lung sq. cell carcinoma (M)	(Wistuba et al., 1999)	RRID:CVCL_5137
Human - HCC1313 Lung sq. cell carcinoma (M)	(Wistuba et al., 1999)	RRID:CVCL_L087
Human - HCC1588 Lung sq. cell carcinoma (F)	(Wistuba et al., 1999)	RRID:CVCL_A351
Human - HCC2814 Lung sq. cell carcinoma (M)	(Gazdar et al., 2010)	RRID:CVCL_V586
Human - NCI-H157 Lung sq. cell carcinoma (M)	ATCC	RRID:CVCL_0463
Human - NCI-H2073 Lung adenocarcinoma (F)	ATCC	RRID:CVCL_1521
Human - DU145 Prostate carcinoma (M)	ATCC	RRID:CVCL_0105
Human - HEK293T (F)	ATCC	RRID:CVCL_0063
Experimental Models: Organisms/Strains		
Mouse: NOD. <i>Cg-Prkdc<sup>scid</sup> Il2rg<sup>tm1Wjl</sup>/SzJ</i> . 4-6-week-old females.	The Jackson Laboratory	Cat. # 005557
Oligonucleotides		
Listed in Table S3.	This paper	N/A
Recombinant DNA		
pENTR221-TMPRSS11B	ThermoFisher	IOH35719
pENTR221-Basigin	ThermoFisher	IOH3378
pLX303::Blast <sup>R</sup>	Addgene	Addgene # 25897
pLX303-GFP-V5::Blast <sup>R</sup>	This paper	N/A
pLX303-mCherry::Blast <sup>R</sup>	This paper	N/A
pLX303-TMPRSS11B-D270N-V5::Blast <sup>R</sup>	This paper	N/A
pLX303-TMPRSS11B-S366A-V5::Blast <sup>R</sup>	This paper	N/A
pLX303-TMPRSS11B-WT-V5::Blast <sup>R</sup>	This paper	N/A
pLX303-TMPRSS11B-WT-HA::Blast <sup>R</sup>	This paper	N/A
pLX307::mCherry	This paper	Addgene 25897 with mCherry instead of Blast <sup>R</sup>
pLX307-Basigin-V5::mCherry	This paper	N/A
pLX307-Basigin-CRISPR-resistant: Synonymous mutations to residues in sgRNA binding site 2, 6, and 9nt from PAM	This paper	N/A
pLentiCRISPRv2::GFP	This paper	Addgene 52961 with GFP instead of Puro <sup>R</sup>
pLentiCRISPRv2::GFP-sgNS (non-specific)	This paper	N/A

REAGENT or RESOURCE	SOURCE	IDENTIFIER
pLentiCRISPRv2::GFP-sg <i>BSG-1</i>	This paper	N/A
pLentiCRISPRv2::GFP-sg <i>BSG-2</i>	This paper	N/A
pLentiCRISPRv2::GFP-sg <i>SLC16A3</i>	This paper	N/A
pLentiCRISPRv2::Puro <sup>R</sup>	Addgene	Addgene 52961
pLentiCRISPRv2::Puro <sup>R</sup> -sgNS (non-specific)	This paper	N/A
pLentiCRISPRv2::Puro <sup>R</sup> -sg <i>TMPRSS11B-1</i>	This paper	N/A
pLentiCRISPRv2::Puro <sup>R</sup> -sg <i>TMPRSS11B-2</i>	This paper	N/A
pTRIPZ::Puro <sup>R</sup>	Dharmacon	Cat. # RHS4696
pTRIPZ-sh <i>TMPRSS11B</i> ::Puro <sup>R</sup>	This paper	N/A
pMD2.G	Addgene	Addgene 12259
psPAX2	Addgene	Addgene 12260
Software and Algorithms		
GraphPad Prism 7	GraphPad Software Inc	<a href="https://www.graphpad.com/scientific-software/prism/">https://www.graphpad.com/scientific-software/prism/</a>
ImageJ	NIH	<a href="https://imagej.nih.gov/ij">https://imagej.nih.gov/ij</a>
Excel	Microsoft	<a href="https://products.office.com/en-us/excel">https://products.office.com/en-us/excel</a>
FlowJo 10.5.3	FlowJo, LLC	<a href="https://www.flowjo.com">https://www.flowjo.com</a>
Fastqc	Babraham Bioinformatics	<a href="http://www.bioinformatics.babraham.ac.uk/projects/fastqc/">http://www.bioinformatics.babraham.ac.uk/projects/fastqc/</a>
Fastq Screen	Babraham Bioinformatics	<a href="http://www.bioinformatics.babraham.ac.uk/projects/fastq_screen">http://www.bioinformatics.babraham.ac.uk/projects/fastq_screen</a>
Fastq-mcf	ea-utils	<a href="https://expressionanalysis.github.io/ea-utils/">https://expressionanalysis.github.io/ea-utils/</a>
TopHat	(Kim and Salzberg, 2011)	N/A
picard-tools	Broad Institute	<a href="https://broadinstitute.github.io/picard/">https://broadinstitute.github.io/picard/</a>
featureCounts	(Liao et al., 2014)	N/A
edgeR	(Robinson et al., 2010)	N/A
Monte-Carlo CIS Simulation	(Guo et al., 2016)	N/A

## CONTACT FOR REAGENT AND RESOURCE SHARING

Further information and requests for resources used in this paper should be directed to the Lead Contact, Kathryn O'Donnell at Kathryn.ODonnell@UTSouthwestern.edu

## EXPERIMENTAL MODEL AND SUBJECT DETAILS

### Animals and xenograft assays

All procedures involving mice were performed in accordance with the recommendations of the Panel on Euthanasia of the American Veterinary Medical Association and protocols approved by the UT Southwestern Institutional Animal Care and Use Committee (protocol # 2017-102112). Cells were trypsinized, counted, resuspended in HBSS-, and injected subcutaneously at 4–5  $\times 10^6$  cells per flank onto both flanks of 4–6-week-old female NOD.*Cg-Prkdc<sup>scid</sup>I12rg<sup>tm1Wjl</sup>/SzJ* (NSG) mice. For inducible shRNA experiments, 2g/L doxycycline hyclate (Sigma, Cat. No. D9891) and 1.5% w/v sucrose was supplied in drinking water *ad libitum*. Tumors were measured every 3–4 days using digital calipers in two perpendicular directions with width measurements being the smaller of the two measurements. Tumor volume was calculated with the formula: volume (mm<sup>3</sup>) =

$(\text{length} \times (\text{width}^2))/2$ . At the end of the experiment, mice were euthanized and excised tumors photographed. Tumor fragments were stored in 10% neutral buffered formalin or snap-frozen in liquid nitrogen. *TMPRSS11B* CRISPR clone 3 was used for tumorigenesis experiments shown in Figure 1H.

## METHOD DETAILS

**Tissue culture and cell lines**—Lung squamous cell carcinomas (HCC95 (M), HCC1313 (M), HCC1588 (F), HCC2814 (M), and H157(M)), lung adenocarcinoma (H2073 (F)), and prostate carcinoma (DU145 (M)) cells were cultured in ATCC-formulated RPMI-1640 with 5% FBS and antibiotic-antimycotic (ThermoFisher Cat. Nos. A1049101 and 15240112, Sigma Cat. No. F2442) (Wistuba et al., 1999; Gazdar et al., 2010). Human bronchial epithelial cells with stable knockdown of TP53 (HBEC-shp53) and all derivatives were cultured in keratinocyte serum-free media (KSFM, ThermoFisher Cat. No. 17005042) with antibiotic-antimycotic and supplied supplements (Ramirez et al., 2004). All cell lines used in this study were cultured in 5% CO<sub>2</sub> at 37C, tested negative for mycoplasma contamination, and have been authenticated using PowerPlex (Promega).

**Soft agar colony formation assays**—Complete medium with 25% v/v FBS, antibiotic-antimycotic, and sterile agarose (SeaKem LE Agarose, Cat. No. 50004) added to 0.5% (bottom layer) and 0.37% (top layer) was added to 12-well plates and  $1 \times 10^3$  cells were added per well. Cells were cultured in 5% CO<sub>2</sub> at 37C with fresh medium with 5% FBS added every three days for the duration of the experiment. Large colonies were quantified 3 weeks after plating.

**Lentivirus and plasmids**—*TMPRSS11B*<sup>D270N</sup> and *TMPRSS11B*<sup>S366A</sup> mutant constructs were generated with Phusion site-directed mutagenesis (ThermoFisher) of IOH35719 (pENTR221, Invitrogen Ultimate ORF collection). *TMPRSS11B*, GFP, or mCherry were cloned into pLX303 (25897, Addgene) using Gateway LR clonase II (Invitrogen, Cat. No. 11791100). For *BSG* and *SLC16A3* knock-out, sgRNAs (Table S3, oligonucleotides) were cloned into pLentiCRISPRv2 modified to express GFP. Single GFP<sup>+</sup> cells were sorted into 96-well plates and expanded for further study. For Basigin rescue experiments, Basigin (IOH3378, Invitrogen Ultimate ORF collection) was modified by site-directed mutagenesis to introduce synonymous mutations to sgRNA binding residues at 2, 6, and 9nt from the PAM and cloned into pLX307 (pLX303 modified to express mCherry instead of a Blast<sup>R</sup> cassette) using Gateway LR clonase II. Following transduction mCherry<sup>+</sup> cells were collected by FACS.

For *TMPRSS11B* knock-out, sgRNAs were cloned into pLentiCRISPRv2-Puro. *TMPRSS11B*-specific shRNA (Table S3, oligonucleotides) was cloned into pTRIPZ (Dharmacon, Cat. No. RHS4696). All lentiviral vectors were packaged in HEK293T cells by co-transfection with packaging plasmids pMD2.G (Addgene, 12259) and psPAX2 (Addgene, 12260) using Effectene transfection reagent (QIAGEN Cat. No. 301427). Conditioned media was taken 48 and 72 hours post transfection, clarified of cells and debris, concentrated with Lenti-X following the manufacturer's protocol (Clontech, Cat. No. 631231), and resuspended in Hank's balanced salt solution (HBSS) (Invitrogen, Cat. No. 14175095).

Recipient cells were transduced in the presence of 8 mg/mL hexadimethrine bromide for 5–8 hours. Transduced cells were selected with either Blasticidin (2–5 mg/mL), Puromycin (1.5–3 mg/mL), or collected FACS on a BD FACSAria II (GFP and mCherry selection).

**[1,6-<sup>13</sup>C] glucose tracing**— $3 \times 10^5$  HCC2814 cells with control or *TMPRSS11B* shRNA were plated in 6-well plates, cultured overnight, and exchanged into glucose- and bicarbonate-free RPMI-1640 with 4.5g/L [1,6-<sup>13</sup>C] glucose and 2g/L NaHCO<sub>3</sub> added. Small aliquots of media were taken at t = 0, 5 m, 15 m, 30 m, and 60 m after media exchange, clarified of debris, and stored at 80C. At the last time point, cells were washed on ice in cold saline solution, scraped into 50% methanol, and transferred to 80C for subsequent analysis. We used a previously described GC-MS protocol (DeNicola et al., 2015) with the aforementioned culture conditions. Cells were lysed in RIPA to determine protein content, and lactate secretion rates were determined by normalizing the lactate abundance in the medium to cellular protein in each well.

**Lactate assays**—Cells were washed twice in cold HBSS- and scraped on ice. Following centrifugation at 1,500 RPM for 5 m at 4 C, cells were resuspended in 500 mL Lactate Assay Buffer (Sigma, Cat. No. MAK064) and acoustically lysed in a BioRuptor for 20 m of 1 m on/off sonication on high at 4 C. Insoluble material was pelleted at 14,000xg for 5 m and supernatant transferred to Amicon Ultra 0.5mL 10K MWCO columns and centrifuged at 14,000xg for 20 m to remove endogenous LDH. Undiluted filtrate was analyzed according to the manufacturer's protocol.

**Seahorse XFe96 assays**— $1.5 \times 10^4$  HBEC cells were plated in a Seahorse XFe 96-well culture plate in KSFM. Glucose, oligomycin, and SR13800 (or DMSO) were loaded into injection wells of an XFe96 cartridge to achieve final concentrations of 10mM, 2 mM, and 5nM, respectively. At the start of the experiment, cells were washed and exchanged into L-15 media without glucose or bicarbonate and run through 4 cycles of 3 minute mix / 3 minute measure per injectant, with the latter 3 measurements being used for data analysis and representation. Bicarbonate- and glucose-free Dulbecco's modified eagle media (DMEM) yielded similar results.

**RT-qPCR**—Cells with inducible shRNA were cultured in 2 mg/mL dox for > 3 days with fresh dox added every 2 days. Cells were washed in cold HBSS-, scraped on ice into HBSS-, and centrifuged at 1,500RPM for 5 m at 4C. Cell pellets were resuspended in 600 mL RLT buffer with fresh b-mercaptoethanol, vortexed, transferred to a QiaShredder column, and centrifuged at max speed for 2 m at 4C. RNA was then extracted according to the RNeasy protocol (QIAGEN) with on-column DNase digest and resuspended in 50 mL nuclease-free H<sub>2</sub>O. RNA (1 mg) served as template for reverse transcription with SuperScript IV VILO (Invitrogen, Cat. No. 11756050). TaqMan probes (Invitrogen) corresponding to *TMPRSS11B* (Hs01113515 m1 and Hs00699337 m1), *BSG* (Hs00936295\_m1), and *GAPDH* (Hs03929097) were used to detect transcripts in 384-well format, and expression calculating using the 2<sup>ddCt</sup> method.

**RNA sequencing**—Cells were plated in triplicate in 15cm<sup>2</sup> dishes and allowed to reach 70% confluence. Cells were then washed in cold HBSS- twice and scraped on ice into

HBSS-. Cells were pelleted at 1,500RPM for 5 m at 4C and resuspended in 600 mL RLT buffer with fresh b-mercaptoethanol, vortexed, transferred to a QiaShredder column, and centrifuged at max speed for 2 m at 4C. RNA was then extracted according to the RNeasy protocol (QIAGEN) with on-column DNase digest and resuspended in 50 mL nuclease-free H<sub>2</sub>O. Samples were run on the Agilent 2100 Bioanalyzer to evaluate RNA quality and were quantified by Qubit (Invitrogen) prior to starting library prep. Four micrograms of total DNase treated RNA were prepared with the TruSeq Stranded Total RNA LT Sample Prep Kit from Illumina. Poly-A RNA was purified and fragmented before strand specific cDNA synthesis. cDNA were A-tailed and indexed adapters were ligated. Samples were then PCR amplified and purified with AmpureXP beads, and validated again on the Agilent 2100 Bioanalyzer. Sequencing was performed on an Illumina NextSeq 500 to generate 76-bp single-ended reads.

**2-NBDG uptake assay**—Cells were washed in warm HBSS- and exchanged into glucose- and bicarbonate-free RPMI1640 media with 5% FBS, antibiotic-antimycotic, 2g/L NaHCO<sub>3</sub>, +/- 50 mM 2-NBDG (Fisher, Cat. No. N13195). After incubation for 30 m at 37C, cells were washed twice in warm HBSS-, trypsinized, resuspended in cold FACS buffer, and 2-NBDG uptake was assessed using a BD Accuri benchtop flow cytometer in the FL-1 channel.

**sReceptor Proteome Profiler Array**—Conditioned media was taken from 75% confluent HBEC-shp53-GFP and HBEC-shp53-TMPRSS11B cells, debris pellet at 1,500xg for 10 m, and supernatant used as substrate for the immobilized antibody array following the manufacturer's protocol (119 factors, sReceptor Proteome Profiler, R&D Systems, Cat. No. ARY012). Developed arrays were scanned and pixel density was quantitated using ImageJ software.

**Basigin ELISA**—For conditioned media quantitation, media was taken and clarified of cells and debris by pelleting at 1,500xg for 10 m. HALT protease and phosphatase inhibitor cocktail (ThermoFisher, Cat. No. 78443) was added to the supernatant and assayed immediately according to the manufacturer's protocol (R&D systems, Human EMMPRIN/CD147 Quantikine ELISA kit, Cat. No. DEMP00). For cellular Basigin quantitation, cells were washed in cold HBSS- after conditioned media collection, scraped on ice into HBSS-, and cells pelleted at 1,500RPM for 5 m at 4C. Cell pellets were resuspended in non-denaturing lysis buffer (LB-17, R&D systems) with protease/phosphatase inhibitors and acoustically lysed using a BioRuptor Plus (Diagenode) at 1 m on/off sonication cycle for 20 m on high at 4C. Insoluble material was pelleted at 14,000xg for 5 m at 4C and supernatant transferred to a clean tube for immediate analysis according to the manufacturer's protocol. Basigin solubilization was calculated as ([soluble Basigin] / [cellular Basigin]).

**Western blotting**—Cells were washed and scraped on ice into HBSS-, pelleted at 1,500 RPM for 5 m at 4C, and resuspended in LB-17 with HALT pro-tease inhibitor cocktail (ThermoFisher, Cat. No. 78443). Cells were acoustically ruptured in a Bioruptor for 15 m of 1 m on/off on high, or in some instances lysed using a QiaShredder column. Insoluble material was pelleted at 14,000xg for 5 m at 4C and supernatant was transferred to a clean tube. Protein concentration of samples was determined by BCA assay (23227,

ThermoFisher). 10–30 mg total protein was combined with 4X LDS loading buffer (NP0008, ThermoFisher) and 10X reducing agent (B0009, ThermoFisher), heated to 70C for 10 m, and loaded into 4%–12% or 10% polyacrylamide SDS gels. Electrophoresed protein was transferred to nitro-cellulose membranes using semi-dry transfer (iBlot II, Invitrogen) then blocked and probed in TBST with 5% w/v milk. A detailed list of antibodies used in this study can be found in the Key Resources Table.

**Immunoprecipitation**—Cells were plated in 15cm<sup>2</sup> dishes and cultured to 70% confluence. Cells were washed twice in cold HBSS- on ice, scraped into cold HBSS-, and pelleted at 1,500 RPM for 5 m at 4C. Cell pellets were resuspended and lysed and immunoprecipitated following the manufacturer’s protocol (Dynabeads Protein G Immunoprecipitation Kit, Cat. No. 10007D) using 5 mg of antibody. Western blots were probed with antibodies of a different host species than what was used for immunoprecipitation.

**Immunofluorescence and confocal microscopy**—Cells were seeded in 6-well plates with UV-sterilized glass coverslips. Cells were washed in PBS and fixed with 4% paraformaldehyde in PBS for 20 min. at room temperature. Cells were washed 3×10 minutes in PBS, blocked with 2% BSA in PBS for 1 hour at room temperature, and then incubated with primary antibodies (1:100 dilution) at 4 C overnight. Cells were washed 3×10 minutes in PBS and incubated in Alexa Flour-conjugated secondary antibodies (CST, 1:500 dilution; Anti-Mouse Alexa Flour 488, Anti-Mouse Alexa Flour 594, Anti-Rabbit Alexa Flour 488, Anti-Rabbit Alexa Flour 594 and Anti-Rat Alexa Flour 647) in 2%BSA in PBS for 2 hours at room temperature. Coverslips with cells were mounted on Fisherbrand Superfrost Plus microscope slides with VECTASHIELD hard set mounting media with DAPI (Vector Labs). All images were captured using a ZEISS LSM-700 confocal microscope.

## QUANTIFICATION AND STATISTICAL ANALYSIS

**GC/MS Metabolite Tracing**—Mass spectrometry and mathematical corrections were performed according to previously established protocols (DeNicola et al., 2015).

**RNA-Seq analysis methods**—Fastq files were checked for quality using fastqc (<http://www.bioinformatics.babraham.ac.uk/projects/fastqc>) and fastq screen ([http://www.bioinformatics.babraham.ac.uk/projects/fastq\\_screen](http://www.bioinformatics.babraham.ac.uk/projects/fastq_screen)) and were quality trimmed using fastq-mcf (Aronesty, 2013). Trimmed fastq files were mapped to hg19 (UCSC version from igenomes) using TopHat (Kim and Salzberg, 2011), duplicates were marked using picard-tools (<https://broadinstitute.github.io/picard/>), read counts were generated using featureCounts (Liao et al., 2014) and differential expression analysis was performed using edgeR (Robinson et al., 2010).

**GraphPad Prism 7**—All growth curves, column graphs, and XY graphs were generated using GraphPad Prism 7 after data normalization and organization in Microsoft Excel. Detailed statistical analyses are listed in figure legends where applicable.

## DATA AND SOFTWARE AVAILABILITY

**RNA sequencing raw and analyzed data**—The accession number for the gene expression data reported in this paper is NCBI GO: GSE114850.

## Supplementary Material

Refer to Web version on PubMed Central for supplementary material.

## ACKNOWLEDGMENTS

We thank the McDermott Center Sequencing and Bioinformatics Cores for sequencing and analysis, Jose Cabrera for assistance with figures, Michael Peyton for sharing cell lines, and Joshua Mendell and members of the O'Donnell laboratory for critical reading of the manuscript. K.A.O. is a Cancer Prevention Research Institute of Texas (CPRIT) Scholar in Cancer Research and a Kimmel Scholar. The accession number for the RNA-seq data reported in this paper is GEO: GSE114850. B.L.U. was supported by CPRIT (RP140110) and an NIH award (T32GM008203). K.A.O. was supported by the NCI (R01 CA207763 and P50 CA70907), the Sidney Kimmel Foundation (SKF-15-067), the CPRIT (R1101 and RP150676), the Welch Foundation (I-1881), and the LUNGevity Foundation (2015-03). R.J.D. was supported by NCI (R35 CA220449) and CPRIT (RP160089). J.D.M. was supported by NIH (P50 CA70907, Lung Cancer SPORE) and CPRIT (RP110708). C.R.-T. was supported by NIH (5T34GM007821-38).

## REFERENCES

- Achreja A, Zhao H, Yang L, Yun TH, Marini J, and Nagrath D (2017). Exo-MFA—a 13C metabolic flux analysis framework to dissect tumor microenvironment-secreted exosome contributions towards cancer cell metabolism. *Metab. Eng* 43 (Pt B), 156–172. [PubMed: 28087332]
- Arendt BK, Walters DK, Wu X, Tschumper RC, and Jelinek DF (2014). Multiple myeloma cell-derived microvesicles are enriched in CD147 expression and enhance tumor cell proliferation. *Oncotarget* 5, 5686–5699. [PubMed: 25015330]
- Aronesty E (2013). Comparison of sequencing utility programs. *Open Bioinform. J* 7, 1–8.
- Barretina J, Caponigro G, Stransky N, Venkatesan K, Margolin AA, Kim S, Wilson CJ, Lehár J, Kryukov GV, Sonkin D, et al. (2012). The Cancer Cell Line Encyclopedia enables predictive modelling of anticancer drug sensitivity. *Nature* 483, 603–607. [PubMed: 22460905]
- Bonon A (2001). The expression of lactate transporters (MCT1 and MCT4) in heart and muscle. *Eur. J. Appl. Physiol* 86, 6–11. [PubMed: 11820324]
- Bugge TH, Antalis TM, and Wu Q (2009). Type II transmembrane serine proteases. *J. Biol. Chem* 284, 23177–23181. [PubMed: 19487698]
- GTE Consortium (2013). The Genotype-Tissue Expression (GTEx) project. *Nat. Genet* 45, 580–585. [PubMed: 23715323]
- DeBerardinis RJ, Lum JJ, Hatzivassiliou G, and Thompson CB (2008). The biology of cancer: metabolic reprogramming fuels cell growth and proliferation. *Cell Metab* 7, 11–20. [PubMed: 18177721]
- DeNicola GM, Chen PH, Mullarky E, Sudderth JA, Hu Z, Wu D, Tang H, Xie Y, Asara JM, Huffman KE, et al. (2015). NRF2 regulates serine biosynthesis in non-small cell lung cancer. *Nat. Genet* 47, 1475–1481. [PubMed: 26482881]
- Dimmer KS, Friedrich B, Lang F, Deitmer JW, and Broer S (2000). The low-affinity monocarboxylate transporter MCT4 is adapted to the export of lactate in highly glycolytic cells. *Biochem. J* 350, 219–227. [PubMed: 10926847]
- Faubert B, Li KY, Cai L, Hensley CT, Kim J, Zacharias LG, Yang C, Do QN, Doucette S, Burguete D, et al. (2017). Lactate metabolism in human lung tumors. *Cell* 171, 358–371. [PubMed: 28985563]
- Feng J, Yang H, Zhang Y, Wei H, Zhu Z, Zhu B, Yang M, Cao W, Wang L, and Wu Z (2017). Tumor cell-derived lactate induces TAZ-dependent upregulation of PD-L1 through GPR81 in human lung cancer cells. *Oncogene* 36, 5829–5839.

- Fischer K, Hoffmann P, Voelkl S, Meidenbauer N, Ammer J, Edinger M, Gottfried E, Schwarz S, Rothe G, Hoves S, et al. (2007). Inhibitory effect of tumor cell-derived lactic acid on human T cells. *Blood* 109, 3812–3819. [PubMed: 17255361]
- Gallagher SM, Castorino JJ, Wang D, and Philp NJ (2007). Monocarboxylate transporter 4 regulates maturation and trafficking of CD147 to the plasma membrane in the metastatic breast cancer cell line MDA-MB-231. *Cancer Res* 67, 4182–4189. [PubMed: 17483329]
- Gao J, Aksoy BA, Dogrusoz U, Dresdner G, Gross B, Sumer SO, Sun Y, Jacobsen A, Sinha R, Larsson E, et al. (2013). Integrative analysis of complex cancer genomics and clinical profiles using the cBioPortal. *Sci. Signal* 6, p11. [PubMed: 23550210]
- Gazdar AF, Girard L, Lockwood WW, Lam WL, and Minna JD (2010). Lung cancer cell lines as tools for biomedical discovery and research. *J. Natl. Cancer Inst* 102, 1310–1321. [PubMed: 20679594]
- Guo Y, Updegraff BL, Park S, Durakoglugil D, Cruz VH, Maddux S, Hwang TH, and O'Donnell KA (2016). Comprehensive *ex vivo* transposon mutagenesis identifies genes that promote growth factor independence and leukemogenesis. *Cancer Res* 76, 773–786. [PubMed: 26676752]
- Halestrap AP, and Price NT (1999). The proton-linked monocarboxylate transporter (MCT) family: structure, function and regulation. *Biochem. J* 343, 281–299. [PubMed: 10510291]
- Hanahan D, and Weinberg RA (2011). Hallmarks of cancer: the next generation. *Cell* 144, 646–674. [PubMed: 21376230]
- Hensley CT, Faubert B, Yuan Q, Lev-Cohain N, Jin E, Kim J, Jiang L, Ko B, Skelton R, Loudat L, et al. (2016). Metabolic heterogeneity in human lung tumors. *Cell* 164, 681–694. [PubMed: 26853473]
- Hori K, Katayama N, Kachi S, Kondo M, Kadomatsu K, Usukura J, Muramatsu T, Mori S, and Miyake Y (2000). Retinal dysfunction in basigin deficiency. *Invest. Ophthalmol. Vis. Sci* 41, 3128–3133. [PubMed: 10967074]
- Hui S, Ghergurovich JM, Morscher RJ, Jang C, Teng X, Lu W, Esparza LA, Reya T, Le Zhan, Yanxiang Guo J, et al. (2017). Glucose feeds the TCA cycle via circulating lactate. *Nature* 551, 115–118. [PubMed: 29045397]
- Igakura T, Kadomatsu K, Kaname T, Muramatsu H, Fan QW, Miyauchi T, Toyama Y, Kuno N, Yuasa S, Takahashi M, et al. (1998). A null mutation in basigin, an immunoglobulin superfamily member, indicates its important roles in peri-implantation development and spermatogenesis. *Dev. Biol* 194, 152–165. [PubMed: 9501026]
- Izumi H, Torigoe T, Ishiguchi H, Uramoto H, Yoshida Y, Tanabe M, Ise T, Murakami T, Yoshida T, Nomoto M, and Kohno K (2003). Cellular pH regulators: potentially promising molecular targets for cancer chemotherapy. *Cancer Treat. Rev* 29, 541–549. [PubMed: 14585264]
- Kanekura T, Chen X, and Kanzaki T (2002). Basigin (CD147) is expressed on melanoma cells and induces tumor cell invasion by stimulating production of matrix metalloproteinases by fibroblasts. *Int. J. Cancer* 99, 520–528. [PubMed: 11992541]
- Kim D, and Salzberg SL (2011). TopHat-Fusion: an algorithm for discovery of novel fusion transcripts. *Genome Biol* 12, R72. [PubMed: 21835007]
- Kirk P, Wilson MC, Heddle C, Brown MH, Barclay AN, and Halestrap AP (2000). CD147 is tightly associated with lactate transporters MCT1 and MCT4 and facilitates their cell surface expression. *EMBO J* 19, 3896–3904. [PubMed: 10921872]
- Le Floch R, Chiche J, Marchiq I, Naiken T, Ilc K, Murray CM, Critchlow SE, Roux D, Simon MP, and Pouyssegur J (2011). CD147 subunit of lactate/H<sup>+</sup> symporters MCT1 and hypoxia-inducible MCT4 is critical for energetics and growth of glycolytic tumors. *Proc. Natl. Acad. Sci. USA* 108, 16663–16668. [PubMed: 21930917]
- Lee ES, Son DS, Kim SH, Lee J, Jo J, Han J, Kim H, Lee HJ, Choi HY, Jung Y, et al. (2008). Prediction of recurrence-free survival in postoperative non-small cell lung cancer patients by using an integrated model of clinical information and gene expression. *Clin. Cancer Res* 14, 7397–7404. [PubMed: 19010856]
- Li R, Huang L, Guo H, and Toole BP (2001). Basigin (murine EMMPRIN) stimulates matrix metalloproteinase production by fibroblasts. *J. Cell. Physiol* 186, 371–379. [PubMed: 11169976]
- Liao Y, Smyth GK, and Shi W (2014). featureCounts: an efficient general purpose program for assigning sequence reads to genomic features. *Bioinformatics* 30, 923–930.

- Maldonado-Báez L, Cole NB, Krämer H, and Donaldson JG (2013). Microtubule-dependent endosomal sorting of clathrin-independent cargo by Hook1. *J. Cell Biol* 201, 233–247. [PubMed: 23589492]
- Marchiq I, Le Floch R, Roux D, Simon MP, and Pouyssegur J (2015). Genetic disruption of lactate/H<sup>+</sup> symporters (MCTs) and their subunit CD147/BASIGIN sensitizes glycolytic tumor cells to phenformin. *Cancer Res* 75, 171–180. [PubMed: 25403912]
- Marieb EA, Zoltan-Jones A, Li R, Misra S, Ghatak S, Cao J, Zucker S, and Toole BP (2004). Emmprin promotes anchorage-independent growth in human mammary carcinoma cells by stimulating hyaluronan production. *Can-cer Res* 64, 1229–1232.
- Miller GS, Zoratti GL, Murray AS, Bergum C, Tanabe LM, and List K (2014). HATL5: a cell surface serine protease differentially expressed in epithelial cancers. *PLoS ONE* 9, e87675. [PubMed: 24498351]
- Millimaggi D, Mari M, D’Ascenzo S, Carosa E, Jannini EA, Zucker S, Carta G, Pavan A, and Dolo V (2007). Tumor vesicle-associated CD147 modulates the angiogenic capability of endothelial cells. *Neoplasia* 9, 349–357. [PubMed: 17460779]
- Philp NJ, Ochrietor JD, Rudoy C, Muramatsu T, and Linser PJ (2003). Loss of MCT1, MCT3, and MCT4 expression in the retinal pigment epithelium and neural retina of the 5A11/basigin-null mouse. *Invest. Ophthalmol. Vis. Sci* 44, 1305–1311. [PubMed: 12601063]
- Quennet V, Yaromina A, Zips D, Rosner A, Walenta S, Baumann M, and Mueller-Klieser W (2006). Tumor lactate content predicts for response to fractionated irradiation of human squamous cell carcinomas in nude mice. *Radiother. Oncol* 81, 130–135. [PubMed: 16973228]
- Ramirez RD, Sheridan S, Girard L, Sato M, Kim Y, Pollack J, Peyton M, Zou Y, Kurie JM, Dimaio JM, et al. (2004). Immortalization of human bronchial epithelial cells in the absence of viral oncoproteins. *Cancer Res* 64, 9027–9034. [PubMed: 15604268]
- Robinson MD, McCarthy DJ, and Smyth GK (2010). edgeR: a Bio-conductor package for differential expression analysis of digital gene expression data. *Bioinformatics* 26, 139–140. [PubMed: 19910308]
- Sato M, Larsen JE, Lee W, Sun H, Shames DS, Dalvi MP, Ramirez RD, Tang H, DiMaio JM, Gao B, et al. (2013). Human lung epithelial cells progressed to malignancy through specific oncogenic manipulations. *Mol. Cancer Res* 11, 638–650. [PubMed: 23449933]
- Sattler UG, Meyer SS, Quennet V, Hoerner C, Knoerzer H, Fabian C, Yaromina A, Zips D, Walenta S, Baumann M, and Mueller-Klieser W (2010). Glycolytic metabolism and tumour response to fractionated irradiation. *Radiother. Oncol* 94, 102–109. [PubMed: 20036432]
- Sonveaux P, Végran F, Schroeder T, Wergin MC, Verrax J, Rabbani ZN, De Saedeleer CJ, Kennedy KM, Diepart C, Jordan BF, et al. (2008). Targeting lactate-fueled respiration selectively kills hypoxic tumor cells in mice. *J. Clin. Invest* 118, 3930–3942. [PubMed: 19033663]
- Su J, Chen X, and Kanekura T (2009). A CD147-targeting siRNA inhibits the proliferation, invasiveness, and VEGF production of human malignant melanoma cells by down-regulating glycolysis. *Cancer Lett* 273, 140–147. [PubMed: 18778892]
- Ullah MS, Davies AJ, and Halestrap AP (2006). The plasma membrane lactate transporter MCT4, but not MCT1, is up-regulated by hypoxia through a HIF-1alpha-dependent mechanism. *J. Biol. Chem* 281, 9030–9037. [PubMed: 16452478]
- Walenta S, Wetterling M, Lehrke M, Schwickert G, Sundfør K, Rofstad EK, and Mueller-Klieser W (2000). High lactate levels predict likelihood of metastases, tumor recurrence, and restricted patient survival in human cervical cancers. *Cancer Res* 60, 916–921. [PubMed: 10706105]
- Warburg O, Wind F, and Negelein E (1927). The metabolism of tumors in the body. *J. Gen. Physiol* 8, 519–530. [PubMed: 19872213]
- Wistuba II, Bryant D, Behrens C, Milchgrub S, Virmani AK, Ashfaq R, Minna JD, and Gazdar AF (1999). Comparison of features of human lung cancer cell lines and their corresponding tumors. *Clin. Cancer Res* 5, 991–1000. [PubMed: 10353731]
- Xu C, Fillmore CM, Koyama S, Wu H, Zhao Y, Chen Z, Herter-Sprie GS, Akbay EA, Tchaicha JH, Altabel A, et al. (2014). Loss of Lkb1 and Pten leads to lung squamous cell carcinoma with elevated PD-L1 expression. *Cancer Cell* 25, 590–604. [PubMed: 24794706]

- Yoshioka Y, Kosaka N, Konishi Y, Ohta H, Okamoto H, Sonoda H, Nonaka R, Yamamoto H, Ishii H, Mori M, et al. (2014). Ultra-sensitive liquid biopsy of circulating extracellular vesicles using ExoScreen. *Nat. Commun* 5, 3591.
- Yurchenko V, Zybarth G, O'Connor M, Dai WW, Franchin G, Hao T, Guo H, Hung HC, Toole B, Gally P, et al. (2002). Active site residues of cyclophilin A are crucial for its signaling activity via CD147. *J. Biol. Chem* 277, 22959–22965. [PubMed: 11943775]
- Zhao H, Yang L, Baddour J, Achreja A, Bernard V, Moss T, Marini JC, Tudawe T, Seviour EG, San Lucas FA, et al. (2016). Tumor microenvironment derived exosomes pleiotropically modulate cancer cell metabolism. *eLife* 5, e10250. [PubMed: 26920219]
- Zucker S, Hymowitz M, Rollo EE, Mann R, Conner CE, Cao J, Foda HD, Tompkins DC, and Toole BP (2001). Tumorigenic potential of extra-cellular matrix metalloproteinase inducer. *Am. J. Pathol* 158, 1921–1928. [PubMed: 11395366]

**Highlights**

- TMPRSS11B is upregulated in human lung squamous cell carcinoma (LSCC) cells
- TMPRSS11B catalytic activity enhances Basigin solubilization
- Basigin membrane release by TMPRSS11B enhances lactate export
- Inhibition of TMPRSS11B reduces lactate export and impairs tumorigenesis

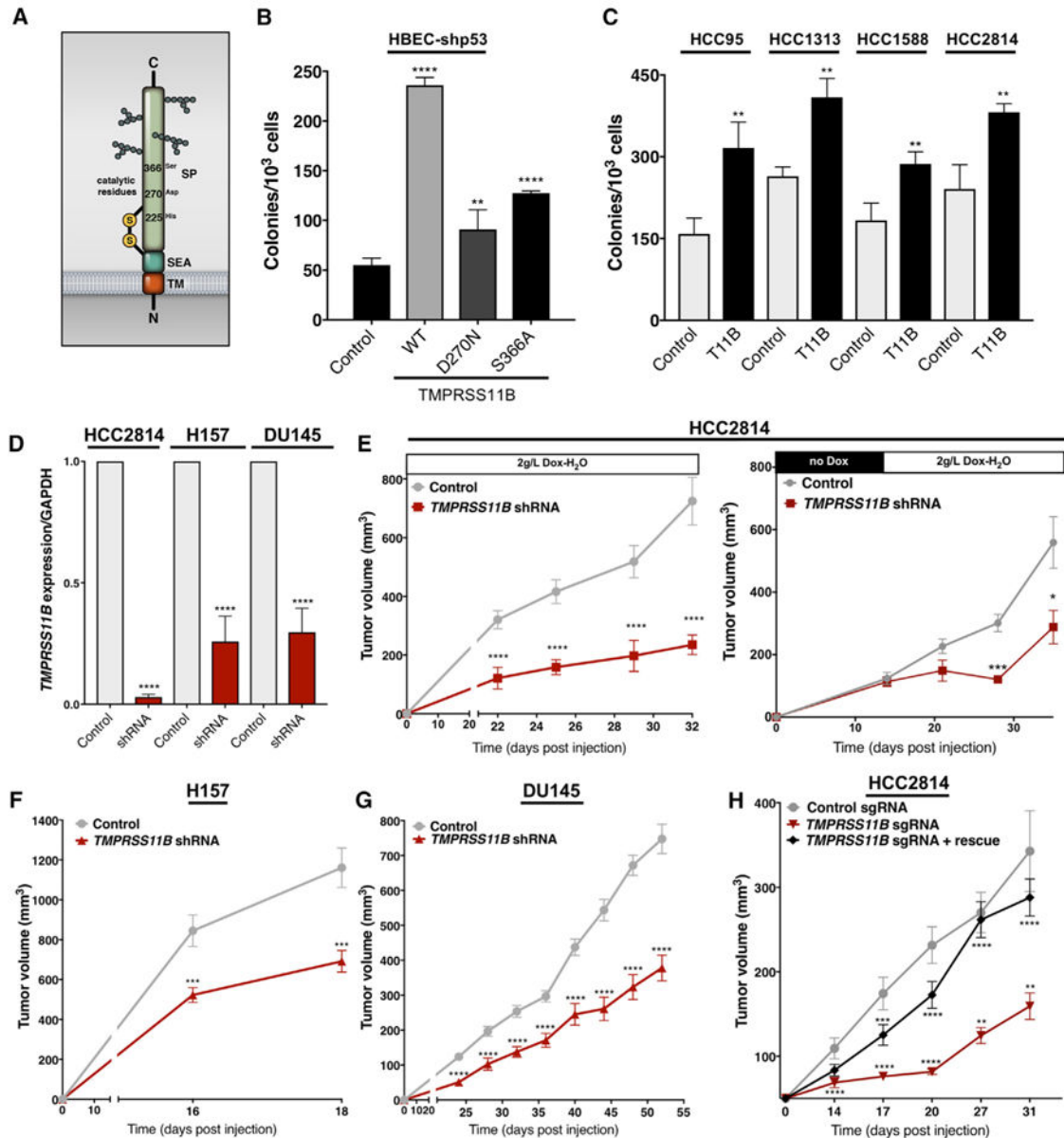


**Figure 1. TMPRSS11B Promotes Transformation *In Vitro* and Tumorigenesis *In Vivo***

(A) Schematic representation of TMPRSS11B with catalytic residues highlighted. TM, transmembrane; SEA, sea urchin sperm protein, aggrecan, and enterokinase domain; SP, serine protease domain.

(B) Soft agar colony formation in human bronchial epithelial cell (HBEC)-shp53 cells expressing GFP (control), D270N and S366A catalytic mutants, or wild-type TMPRSS11B ( $n = 3$ , error bars represent SD).

(C) Soft agar colony formation in SCC lines expressing mCherry (control) or TMPRSS11B ( $n = 3$ , error bars represent SD).

(D) Quantitative real-time PCR verification of *TMPRSS11B* knockdown in cells used for xenograft assays in (E)–(G) ( $n = 3$  for each cell line, error bars represent SD).

(E) TMPRSS11B knockdown blunts subcutaneous tumor growth of HCC2814 cells. (Left) Mice treated with doxycycline (dox) water to induce TMPRSS11B knockdown at the time of injection (n = 16 tumors/group). (Right) Mice treated with dox water when tumors were palpable (n = 6 tumors/group). Error bars represent SEM for both right and left graphs.

(F) TMPRSS11B knockdown inhibits subcutaneous tumor growth of H157 cells (n = 16 tumors/group, error bars represent SEM). Mice were treated with dox water at the time of injection.

(G) TMPRSS11B knockdown reduces subcutaneous tumor growth of DU145 cells (n = 16 tumors/group, error bars represent SEM). Mice were treated with dox water at the time of injection.

(H) CRISPR/Cas9 depletion of TMPRSS11B (sgRNA1 clone 3) blunts tumor growth in HCC2814 cells that is restored upon introduction of a CRISPR-resistant TMPRSS11B cDNA (n = 16 tumors/group, error bars represent SEM).

Unpaired t test; Benjamini, Krieger, and Yekutieli approach; \*p < 0.05, \*\*p < 0.01, \*\*\*p < 0.001, \*\*\*\*p < 0.0001.

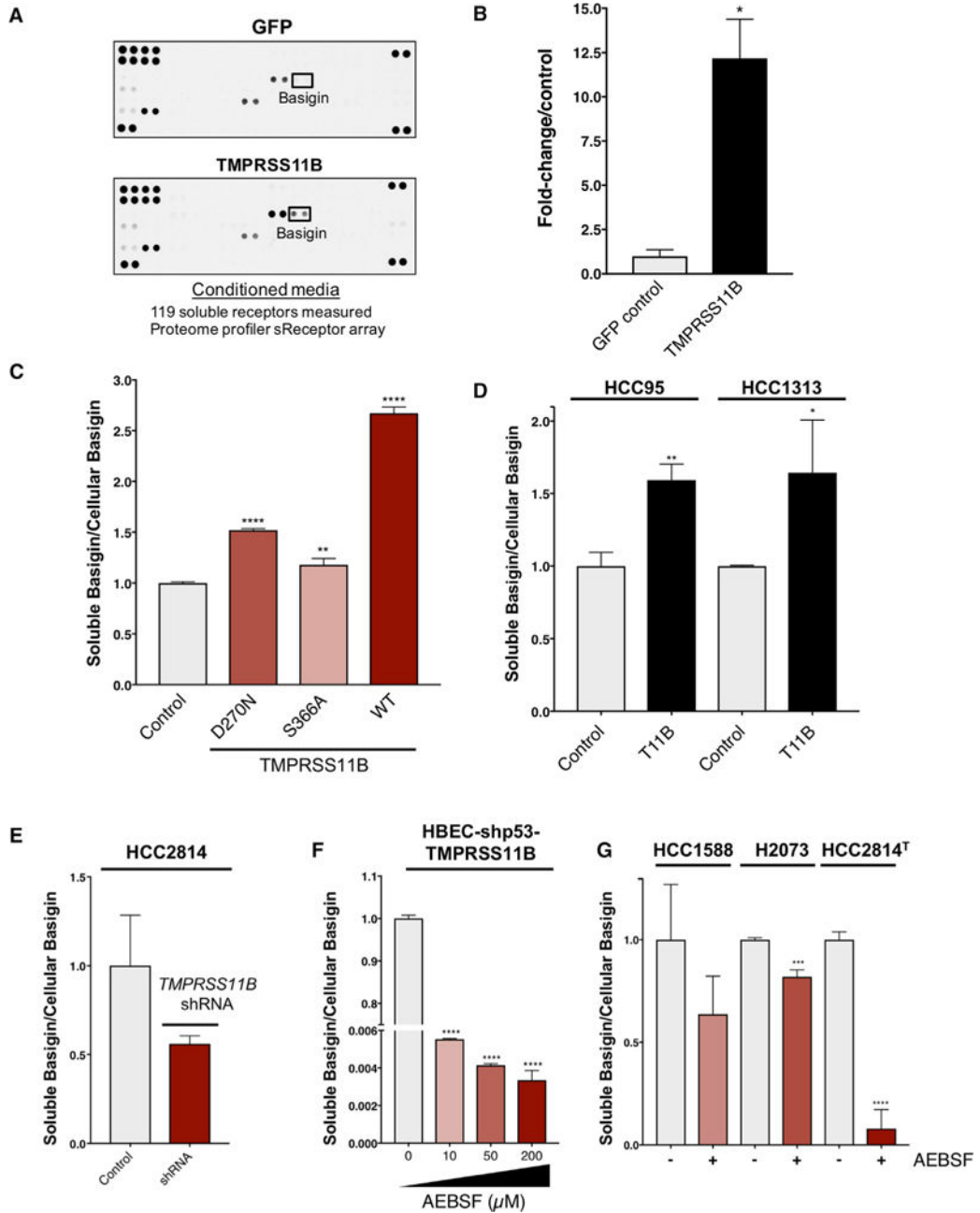


**Figure 2. TMPRSS11B Promotes Basigin Solubilization**

(A) Immobilized antibody array on conditioned media harvested from HBEC-shp53-GFP versus HBEC-shp53-TMPRSS11B cells (119 factors profiled, n = 2).

(B) Pixel density quantitation of array from (A). Data bars represent SD.

(C) Basigin solubilization (conditioned media Basigin:total cellular Basigin) in HBEC-shp53 cells expressing GFP, TMPRSS11B-D270N, TMPRSS11B-S366A, or WT TMPRSS11B (n = 3, error bars represent SD).

(D) TMPRSS11B enhances Basigin membrane release in HCC95 and HCC1313 cells (n = 3, error bars represent SD).

(E) Inducible shRNA depletion of TMPRSS11B reduces Basigin membrane release in HCC2814 cells (n = 3, error bars represent SD).

(F) Treatment of HBEC-shp53 cells with the serine protease inhibitor AEBSF reduces Basigin solubilization (n = 2, error bars represent SD).

(G) Treatment of HCC1588, H2073, and HCC2814<sup>T</sup> (T denotes TMPRSS11B overexpression) with AEBSF reduces Basigin membrane release (n = 3, error bars represent SD).

Unpaired t test; Benjamini, Krieger, and Yekutieli approach; \*p < 0.05, \*\*p < 0.01, \*\*\*p < 0.001, \*\*\*\*p < 0.0001.

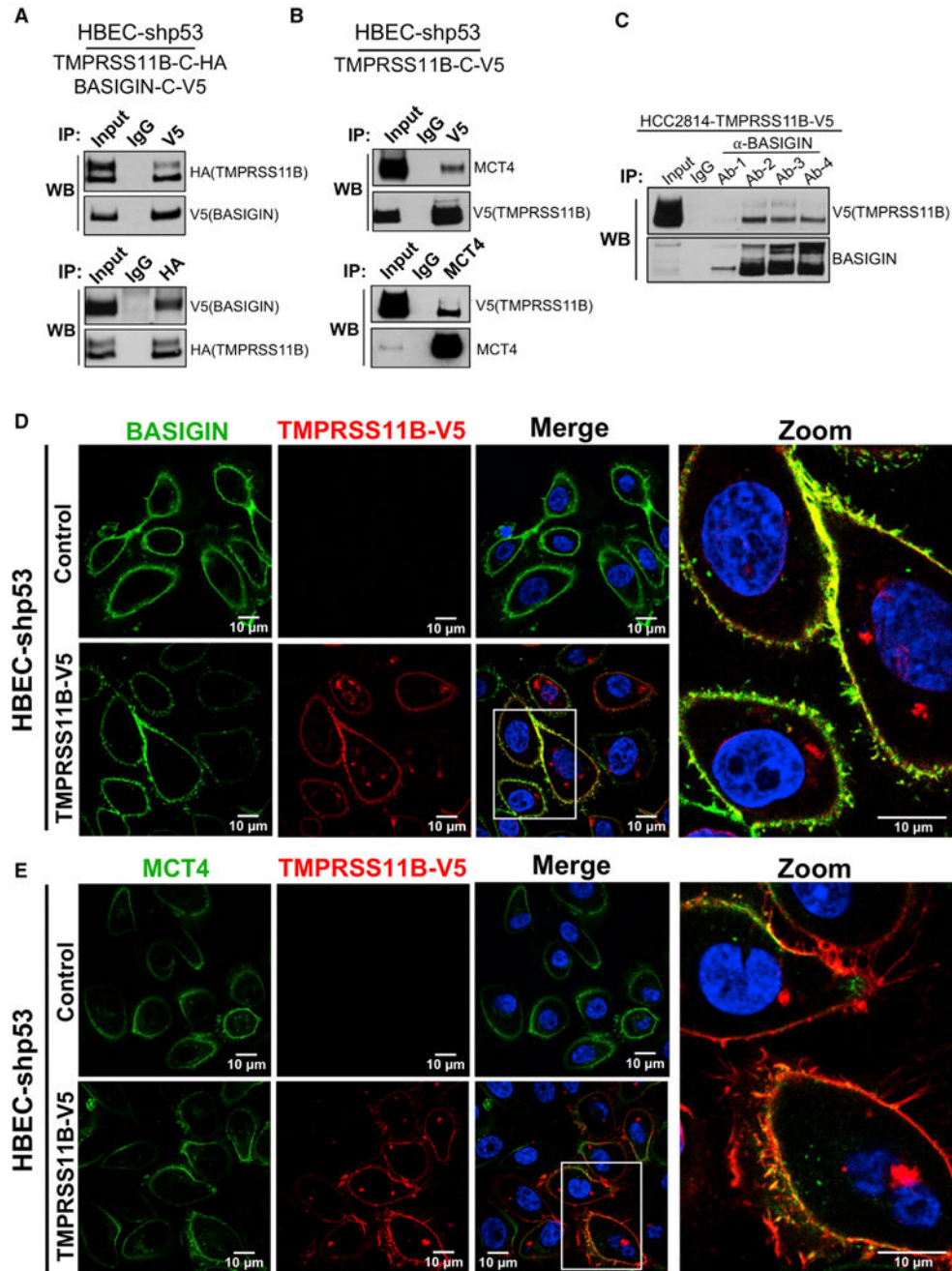


**Figure 3. TMPRSS11B Interacts and Co-localizes with Basigin and MCT4 at the Plasma Membrane**

(A) Reciprocal co-immunoprecipitation (coIP) of HA-tagged TMPRSS11B and V5-tagged Basigin in HBEC-shp53 cells.

(B) Reciprocal coIP of V5-tagged TMPRSS11B and an antibody that recognizes endogenous MCT4 in HBEC-shp53 cells.

(C) CoIP of endogenous Basigin with three independent antibodies reveals interaction with V5-tagged TMPRSS11B.

(D) Immunofluorescence (IF) confocal microscopy of HBEC-shp53-V5-TMPRSS11B cells stained with anti-V5 and anti-Basigin.

(E) IF confocal microscopy of HBEC-shp53-V5-TMPRSS11B cells stained with anti-V5 and anti-MCT4. All slides were mounted in solution containing DAPI.

Author Manuscript

Author Manuscript

Author Manuscript

Author Manuscript

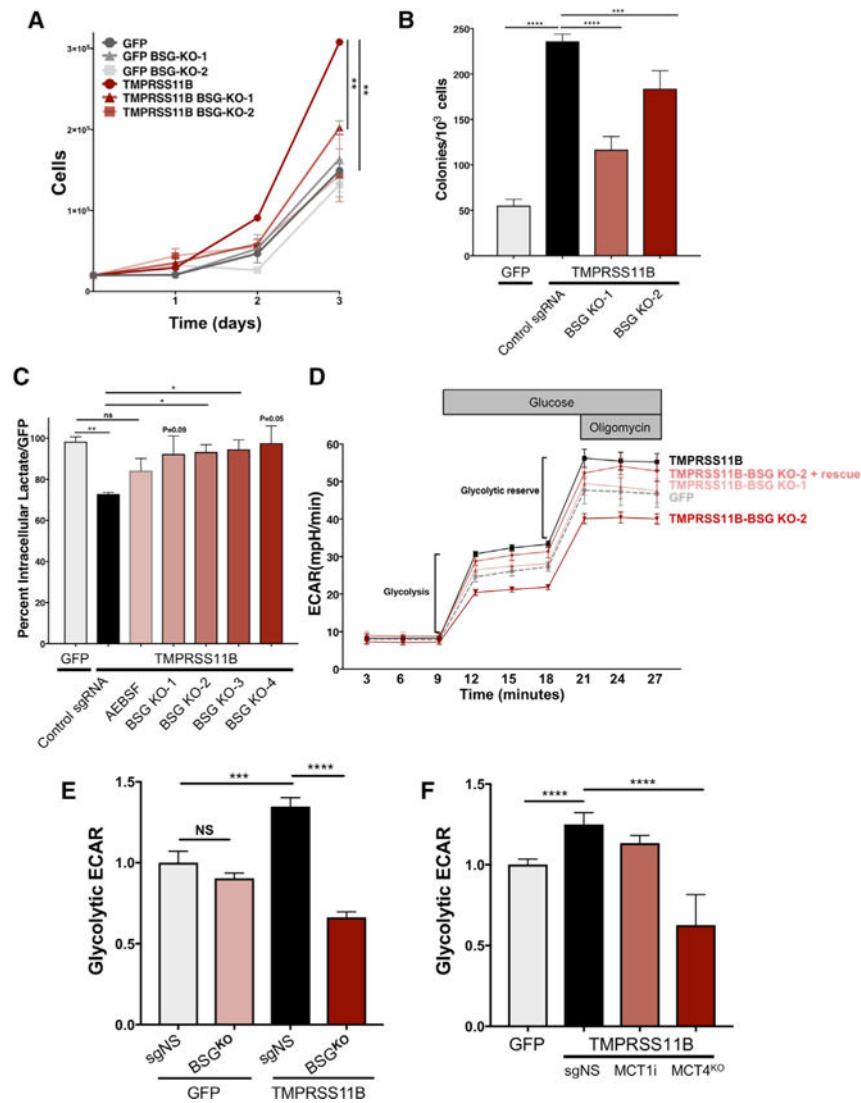


#### Figure 4. TMPRSS11B Regulates Glycolysis and Lactate Export by Enhancing Basigin/ MCT4 Function

(A) Proliferation of isogenic HBEC-shp53 Basigin knockout (KO) clones or sgNS (control non-targeting sgRNA) with either stable GFP or TMPRSS11B expression.

(B) Soft agar quantitation of large colonies in HBEC-shp53-GFP and HBEC-shp53-TMPRSS11B with and without Basigin KO (n = 3, error bars represent SD).

(C) Intracellular lactate quantification in HBEC-shp53 cells reveals a protease- and Basigin-dependent reduction in cellular lactate content (n = 2, error bars represent SD).

(D) SeaHorse analysis of the extracellular acidification rate (ECAR) in  $1.5 \times 10^4$  HBEC-shp53 cells reveals enhanced lactate export in HBEC-shp53-TMPRSS11B relative to HBEC-shp53-GFP cells and HBEC-shp53-TMPRSS11B with Basigin knockout (n = 5–6, error bars represent SEM).

(E) Relative glycolytic ECAR ((ECAR after glucose injection basal ECAR) normalized to HBEC-shp53-sgNS-GFP) of Basigin KO HBEC-shp53 cells expressing GFP or

TMPRSS11B (n = 36 for control sgNS-GFP, n = 72 for experimental groups, error bars represent SEM).

(F) Relative ECAR of MCT4 KO and MCT1 inhibitor-treated HBEC-shp53-TMPRSS11B cells (n = 15–18, error bars represent SEM).

Unpaired t test; Benjamini, Krieger, and Yekutieli approach; \*p < 0.05, \*\*p < 0.01, \*\*\*p < 0.001, \*\*\*\*p < 0.0001.

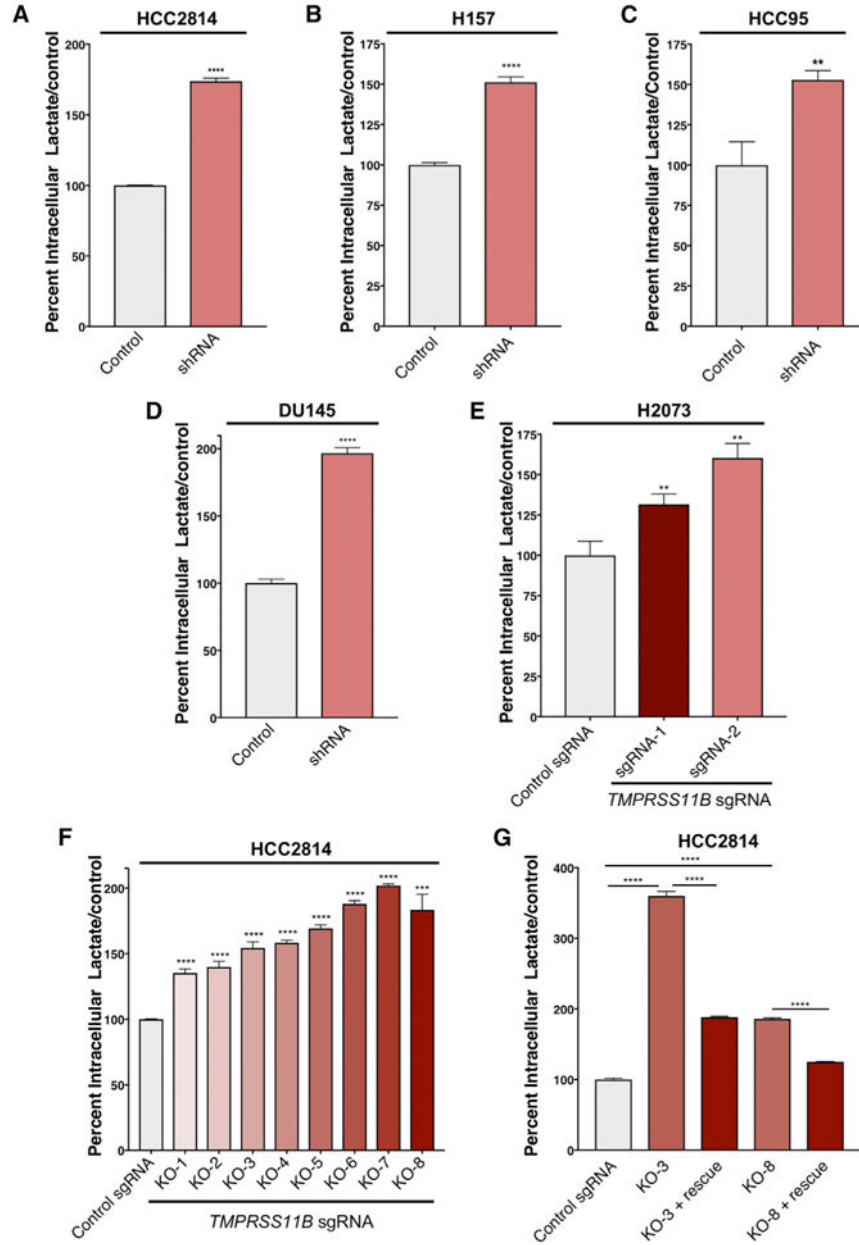


### Figure 5. TMPRSS11B Regulates Cellular lactate Levels

(A–F) Inducible knockdown of TMPRSS11B pro-motes lactate accumulation in HCC2814 (A), H157 (B), HCC95 (C), and DU145 (D) cells. CRISPR/Cas9 depletion of TMPRSS11B results in lactate accumulation in H2073 (E) and HCC2814 (F) cells (n = 3, error bars represent SD).

(G) Lactate accumulation in CRISPR/Cas9-modified HCC2814 cells can be rescued by introduction of a CRISPR-resistant TMPRSS11B cDNA (n = 3, error bars represent SD). Unpaired t test; Benjamini, Krieger, and Yekutieli approach; \*\*p < 0.01, \*\*\*p < 0.001, \*\*\*\*p < 0.0001.

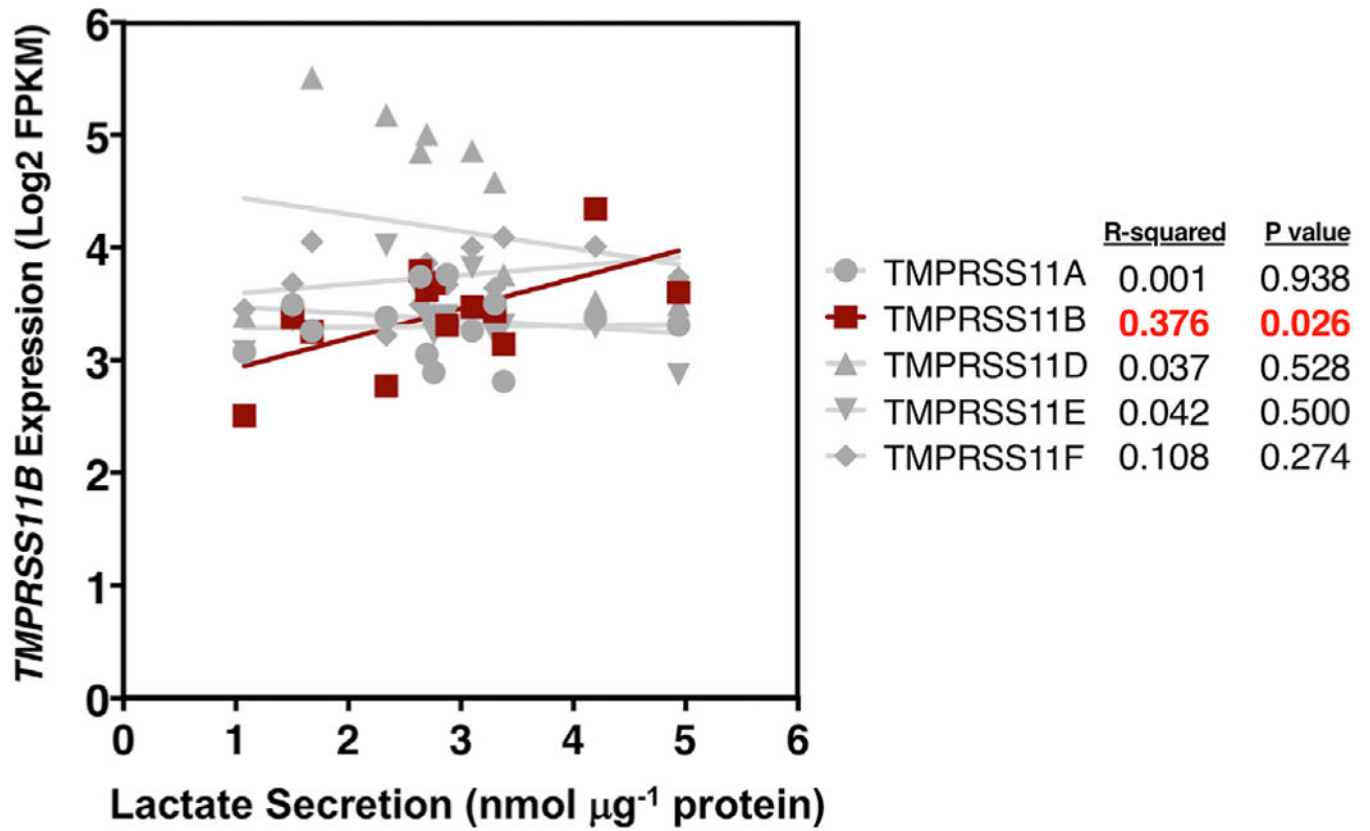


**Figure 6. TMPRSS11B Expression Is Associated with Lactate Secretion in LSCCs**  
*TMPRSS11B* mRNA expression correlates with lactate secretion in human LSCCs (n = 12 cell lines, linear regression and goodness of fit analysis).

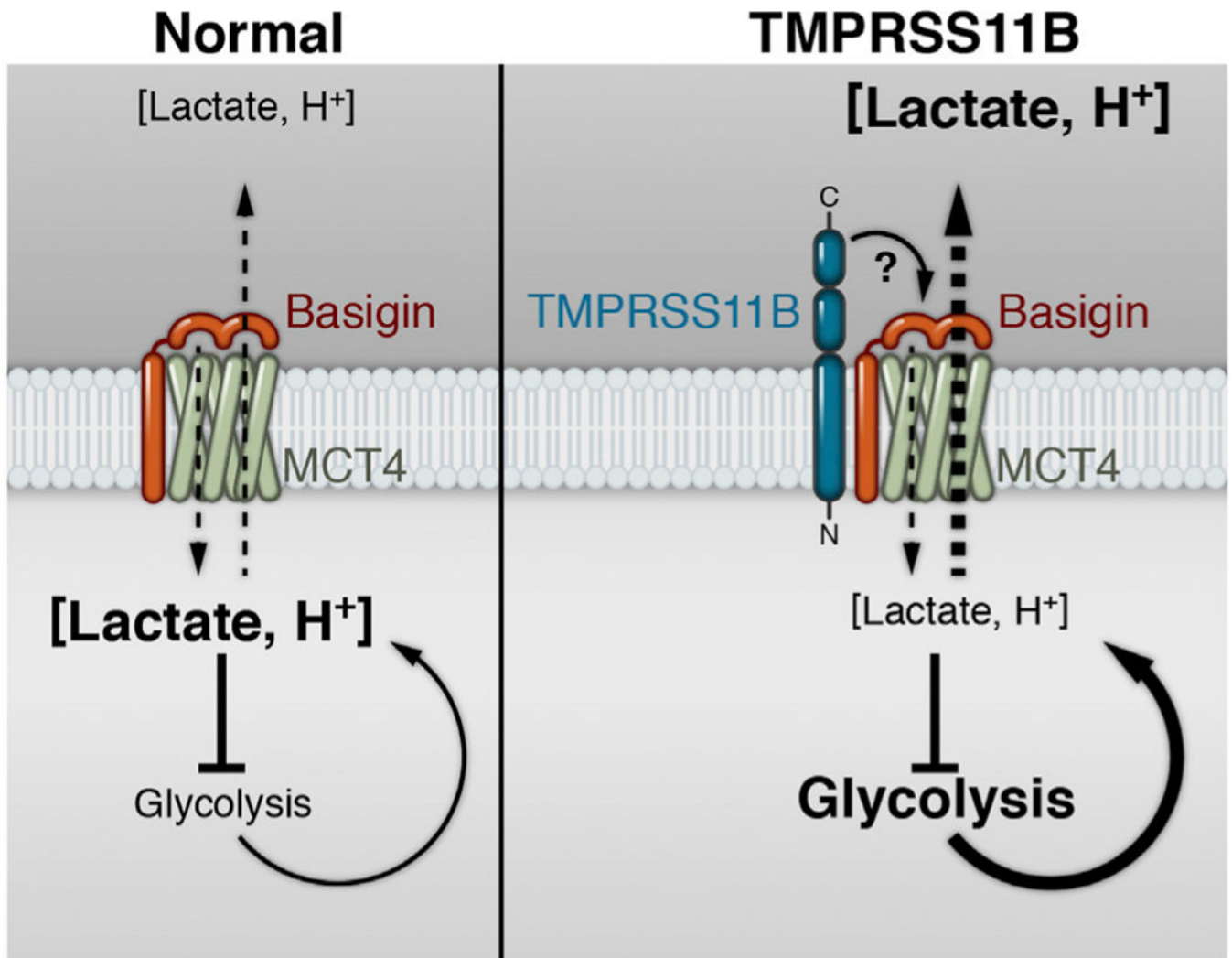


**Figure 7. Model of TMPRSS11B-Mediated Regulation of Lactate Export and Glycolysis**  
 (Left) In healthy lung lacking TMPRSS11B expression, Basigin serves a chaperone role in regulating the efficiency of lactate export through MCT4. (Right) In LSCCs with upregulated expression of TMPRSS11B, solubilization of Basigin enhances lactate export efficiency through MCT4, in turn removing a feedback-regulatory role of cellular lactate on glycolytic flux.

## KEY RESOURCES TABLE

REAGENT or RESOURCE	SOURCE	IDENTIFIER
<b>Antibodies</b>		
Rabbit anti-human Basigin (E1S1V)	Cell Signaling Technology	Cat. # 13287S
Mouse anti-human Basigin (1S9-2A)	Millipore Sigma	Cat. # MAB2623; RRID:AB_11212827
Mouse anti-human Basigin (MEM/M6-6)	Abcam	Cat. # ab119114; RRID:AB_2274970
Mouse anti-human Basigin (MEM/M6-1)	Abcam	Cat. # ab666; RRID:AB_1508093
Mouse anti-human Basigin (MEM/M6-6)	ThermoFisher	Cat. # MA1-10103; RRID:AB_2274970
Rabbit anti-beta-Actin (13E5)	Cell Signaling Technology	Cat. # 4970S
Rabbit anti-HA (C29F4)	Cell Signaling Technology	Cat. # 3724S
Mouse anti-HA (HA-7)	Millipore Sigma	Cat. # H3663; RRID:AB_262051
Rat anti-HA (3F10)	Millipore Sigma	Cat. # 11867423001; RRID:AB_390918
Mouse anti-MCT1 (H-1)	Santa Cruz Biotechnology	Cat. # sc-365501; RRID:AB_10841766
Mouse anti-MCT4 (D-1)	Santa Cruz Biotechnology	Cat. # sc-376140; RRID:AB_10992036
Rabbit anti-MCT4 (polyclonal, Prestige)	Millipore Sigma	Cat. # HPA021451; RRID:AB_1853663
Mouse anti-Tubulin (DM1A)	Abcam	Cat. # ab7291; RRID:AB_2241126
Mouse anti-V5	ThermoFisher	Cat. # R960-25; RRID:AB_2556564
Rabbit anti-V5 (D3H8Q)	Cell Signaling Technology	Cat. # 13202S
Goat anti-mouse-Alexa Flour 488	Cell Signaling Technology	Cat. # 4408S; RRID:AB_2576208
Goat anti-rabbit-Alexa Flour 488	Cell Signaling Technology	Cat. # 4412S; RRID:AB_2630356
Goat anti-rabbit-Alexa Flour 594	Cell Signaling Technology	Cat. # 8889S; RRID:AB_2650602
Goat anti-rat-Alexa Flour 647	Cell Signaling Technology	Cat. # 4418S; RRID:AB_2566823
Horse anti-mouse-IgG HRP secondary	Cell Signaling Technology	Cat. # 7076S
Goat anti-rabbit-IgG HRP secondary	Cell Signaling Technology	Cat. # 7074S
<b>Bacterial and Virus Strains</b>		
OneShot Stbl3 <i>E. coli</i>	ThermoFisher	Cat. # C737303
Lentivirus: LX303	This paper	Addgene 25897
Lentivirus: LX307	This paper	N/A
Lentivirus: LentiCRISPRv2	This paper	Addgene 52961
Lentivirus: TRIPZ	This paper	Cat. # RHS4696
<b>Biological Samples</b>		
Xenograft tumor tissue: HCC2814 Lung sq. cell carcinoma (M)	This paper	Cell line: RRID:CVCL_V586
Xenograft tumor tissue: H157 Lung sq. cell carcinoma (M)	This paper	Cell line: RRID:CVCL_0463
Xenograft tumor tissue: DU145 Prostate carcinoma (M)	This paper	Cell line: RRID:CVCL_0105
<b>Chemicals, Peptides, and Recombinant Proteins</b>		

REAGENT or RESOURCE	SOURCE	IDENTIFIER
SR13800 (MCT1 inhibitor)	Millipore Sigma	Cat. # 509663
Oligomycin	Millipore Sigma	Cat. # 75351
[1,6- <sup>13</sup> C] glucose	Millipore Sigma	Cat. # 453196
Pefabloc SC AEBSF (Serine protease inhibitor)	Millipore Sigma	Cat. # 11429868001
Doxycycline hyclate	Millipore Sigma	Cat. # D9891
Hexadimethrine bromide	Millipore Sigma	Cat. # 107689
Fetal bovine serum (FBS)	Millipore Sigma	Cat. # F2442
Puromycin dihydrochloride	ThermoFisher	Cat. # A1113803
Blasticidin S HCl	ThermoFisher	Cat. # A1113903
2-NBDG	ThermoFisher	Cat. # N13195
HALT Protease Inhibitor Cocktail	ThermoFisher	Cat. # 78430
NuPAGE LDS Sample Loading Buffer	ThermoFisher	Cat. # NP0008
NuPAGE Sample Reducing Agent	ThermoFisher	Cat. # NP0004
Bolt 4–12% Bis-Tris Plus Gels	ThermoFisher	Cat. # NW04120BOX
Phusion Site-Directed Mutagenesis Kit	ThermoFisher	Cat. # F541
Gateway LR Clonase II Enzyme Mix	ThermoFisher	Cat. # 11791100
SuperScript IV VILO RT Master Mix	ThermoFisher	Cat. # 11756050
Hanks Balanced Salt Solution, no magnesium, no calcium, no phenol red (HBSS-)	ThermoFisher	Cat. 14175103
Keratinocyte Serum-Free Medium (KFSM)	ThermoFisher	Cat. # 17005042
RPME-1640 medium	ThermoFisher	Cat. # A1049101
RPME-1640 medium, glucose/bicarbonate-free	ThermoFisher	Cat. # R1383
Leibovitz's L-15 medium, no phenol red	ThermoFisher	Cat. # 21083027
Lysis Buffer LB-17	R&D Systems	Cat. # 895943
Lenti-X Concentrator	Clontech	Cat. # 631232
Effectene Transfection Reagent	QIAGEN	Cat. # 301427
RNeasy Mini Kit	QIAGEN	Cat. # 74106
Critical Commercial Assays		
sReceptor Proteome Profiler Array	R&D Systems	Cat. # ARY012
EMMPRIN/CD147 Quantikine ELISA	R&D Systems	Cat. # DEMP00
Lactate Assay Kit	Millipore Sigma	Cat. # MAK064
TaqMan Universal qPCR Master Mix	ThermoFisher	Cat. # 4304437
Dynabeads Protein G Immunoprecipitation Kit	ThermoFisher	Cat. # 10007D
Pierce BCA Protein Assay Kit	ThermoFisher	Cat. # 23225
SeaKem LE Agarose	Lonza	Cat. # 50004
Deposited Data		
RNA sequencing data and analysis	NCBI GEO	GSE114850
Experimental Models: Cell Lines		
Human – HBEC-3KT (F)	(Ramirez et al., 2004)	RRID:CVCL_EQ78

REAGENT or RESOURCE	SOURCE	IDENTIFIER
Human - HCC95 Lung sq. cell carcinoma (M)	(Wistuba et al., 1999)	RRID:CVCL_5137
Human - HCC1313 Lung sq. cell carcinoma (M)	(Wistuba et al., 1999)	RRID:CVCL_L087
Human - HCC1588 Lung sq. cell carcinoma (F)	(Wistuba et al., 1999)	RRID:CVCL_A351
Human - HCC2814 Lung sq. cell carcinoma (M)	(Gazdar et al., 2010)	RRID:CVCL_V586
Human - NCI-H157 Lung sq. cell carcinoma (M)	ATCC	RRID:CVCL_0463
Human - NCI-H2073 Lung adenocarcinoma (F)	ATCC	RRID:CVCL_1521
Human - DU145 Prostate carcinoma (M)	ATCC	RRID:CVCL_0105
Human - HEK293T (F)	ATCC	RRID:CVCL_0063
Experimental Models: Organisms/Strains		
Mouse: NOD. <i>Cg-Prkdc<sup>scid</sup> Il2rg<sup>tm1Wjl</sup>/SzJ</i> . 4-6-week-old females.	The Jackson Laboratory	Cat. # 005557
Oligonucleotides		
Listed in Table S3.	This paper	N/A
Recombinant DNA		
pENTR221-TMPRSS11B	ThermoFisher	IOH35719
pENTR221-Basigin	ThermoFisher	IOH3378
pLX303::Blast <sup>R</sup>	Addgene	Addgene # 25897
pLX303-GFP-V5::Blast <sup>R</sup>	This paper	N/A
pLX303-mCherry::Blast <sup>R</sup>	This paper	N/A
pLX303-TMPRSS11B-D270N-V5::Blast <sup>R</sup>	This paper	N/A
pLX303-TMPRSS11B-S366A-V5::Blast <sup>R</sup>	This paper	N/A
pLX303-TMPRSS11B-WT-V5::Blast <sup>R</sup>	This paper	N/A
pLX303-TMPRSS11B-WT-HA::Blast <sup>R</sup>	This paper	N/A
pLX307::mCherry	This paper	Addgene 25897 with mCherry instead of Blast <sup>R</sup>
pLX307-Basigin-V5::mCherry	This paper	N/A
pLX307-Basigin-CRISPR-resistant: Synonymous mutations to residues in sgRNA binding site 2, 6, and 9nt from PAM	This paper	N/A
pLentiCRISPRv2::GFP	This paper	Addgene 52961 with GFP instead of Puro <sup>R</sup>
pLentiCRISPRv2::GFP-sgNS (non-specific)	This paper	N/A
pLentiCRISPRv2::GFP-sg <i>BSG-1</i>	This paper	N/A
pLentiCRISPRv2::GFP-sg <i>BSG-2</i>	This paper	N/A
pLentiCRISPRv2::GFP-sg <i>SLC16A3</i>	This paper	N/A
pLentiCRISPRv2::Puro <sup>R</sup>	Addgene	Addgene 52961
pLentiCRISPRv2::Puro <sup>R</sup> -sgNS (non-specific)	This paper	N/A
pLentiCRISPRv2::Puro <sup>R</sup> -sg <i>TMPRSS11B-1</i>	This paper	N/A
pLentiCRISPRv2::Puro <sup>R</sup> -sg <i>TMPRSS11B-2</i>	This paper	N/A
pTRIPZ::Puro <sup>R</sup>	Dharmacon	Cat. # RHS4696

REAGENT or RESOURCE	SOURCE	IDENTIFIER
pTRIPZ-shTMPRSS11B::Puro <sup>R</sup>	This paper	N/A
pMD2.G	Addgene	Addgene 12259
psPAX2	Addgene	Addgene 12260
Software and Algorithms		
GraphPad Prism 7	GraphPad Software Inc	<a href="https://www.graphpad.com/scientific-software/prism/">https://www.graphpad.com/scientific-software/prism/</a>
ImageJ	NIH	<a href="https://imagej.nih.gov/ij">https://imagej.nih.gov/ij</a>
Excel	Microsoft	<a href="https://products.office.com/en-us/excel">https://products.office.com/en-us/excel</a>
FlowJo 10.5.3	FlowJo, LLC	<a href="https://www.flowjo.com">https://www.flowjo.com</a>
Fastqc	Babraham Bioinformatics	<a href="http://www.bioinformatics.babraham.ac.uk/projects/fastqc/">http://www.bioinformatics.babraham.ac.uk/projects/fastqc/</a>
Fastq Screen	Babraham Bioinformatics	<a href="http://www.bioinformatics.babraham.ac.uk/projects/fastq_screen">http://www.bioinformatics.babraham.ac.uk/projects/fastq_screen</a>
Fastq-mcf	ea-utils	<a href="https://expressionanalysis.github.io/ea-utils/">https://expressionanalysis.github.io/ea-utils/</a>
TopHat	(Kim and Salzberg, 2011)	N/A
picard-tools	Broad Institute	<a href="https://broadinstitute.github.io/picard/">https://broadinstitute.github.io/picard/</a>
featureCounts	(Liao et al., 2014)	N/A
edgeR	(Robinson et al., 2010)	N/A
Monte-Carlo CIS Simulation	(Guo et al., 2016)	N/A